Journal of
Ceramic Science
and Technology

J. Ceram. Sci. Tech., 07 [01] 1-28 (2016)
DOI: 10.4416/JCST2015-00025
available online at: http://www.ceramic-science.com

Review

Practical Colloidal Processing of Multication Ceramics

N.S. Bell*[1], T.C. Monson[2], C. DiAntonio[3], Y. Wu[4]

[1]Sandia National Laboratories, 01815 – Advanced Materials Lab, PO Box 5800 MS1411, Albuquerque, NM 87185 USA
[2]Sandia National Laboratories, 01124 – Nanoscale Sciences, PO Box 5800 MS1415, Albuquerque, NM 87185 USA
[3]Sandia National Laboratories, 02734 – Ferroelectric Neutron Generator and Tube Lifecycle Engineering, PO Box 5800 MS0958, Albuquerque, NM 87185 USA
[4]Kazuo Inamori School of Engineering New York State College of Ceramics, Alfred University, 2 Pine Street, Alfred, NY 14802 – 1296, USA

received June 12, 2015; received in revised form August 7, 2015; accepted September 7, 2015

Abstract

The use of colloidal processing principles in the formation of ceramic materials is well appreciated for developing homogeneous material properties in sintered products, enabling novel forming techniques for porous ceramics or 3D printing, and controlling microstructure to enable optimized material properties. The solution processing of electronic ceramic materials often involves multiple cationic elements or dopants to affect microstructure and properties. Material stability must be considered through the steps of colloidal processing to optimize desired component properties. This review provides strategies for preventing material degradation in particle synthesis, milling processes, and dispersion, with case studies of consolidation using spark plasma sintering of these systems. The prevention of multication corrosion in colloidal dispersions can be achieved by utilizing conditions similar to the synthesis environment or by the development of surface passivation layers. The choice of dispersing surfactants can be related to these surface states, which are of special importance for nanoparticle systems. A survey of dispersant chemistries related to some common synthesis conditions is provided for perovskite systems as an example. These principles can be applied to many colloidal systems related to electronic and optical applications.

Keywords: Colloids, ceramic processing, dispersions, spark plasma sintering

I. Introduction

Ceramic components are one of the oldest manufactured materials as exemplified by archaeological pottery artifacts. In the last two centuries, the advances in ceramic component production have vastly expanded the application of these materials in contemporary life, and especially in the role of electronic components for energy storage, transmission, and regulation of power. In many instances these colloidal systems and processes can be categorized as 'advanced ceramics'. They are typically manufactured from materials with very high purity levels and are sintered under strictly controlled profiles and conditions, unlike the more 'traditional ceramic' products such as flooring, wall tile, pottery, china, refractory brick, etc. This results in specifically tailored microscopic/macroscopic properties that are critical to the proper performance of the component in application. The final macroscopic properties therefore are intimately tied to the chemical composition of the material (based on the intrinsic properties), atomic structure, processing parameters, and microstructure of the polycrystalline ceramic, as illustrated in Fig. 1. Overall the final quality of these advanced ceramics is of grave concern and is typically addressed and maintained at a high level through colloidal synthesis and processing, more exact product forming by employing near-net shape techniques and improved sintering control, prediction and modeling.

Colloidal synthesis and processing typically requires an intimate control of solution chemistry and the dispersion of particles in aqueous or non-aqueous suspensions, which can then be formed into the desired shape. The concept requires the control and manipulation of interparticle forces in the suspension to create a colloidally stable environment, where ideally every particle is separated from one another [1]. This offers significant advantages that usually cannot be fully realized in more traditional particle processing, including reducing inhomogeneities in the green microstructure by minimizing agglomeration, increasing the packing density and uniformity, and narrowing the pore size distribution [2–4].

* Corresponding author: nsbell@sandia.gov

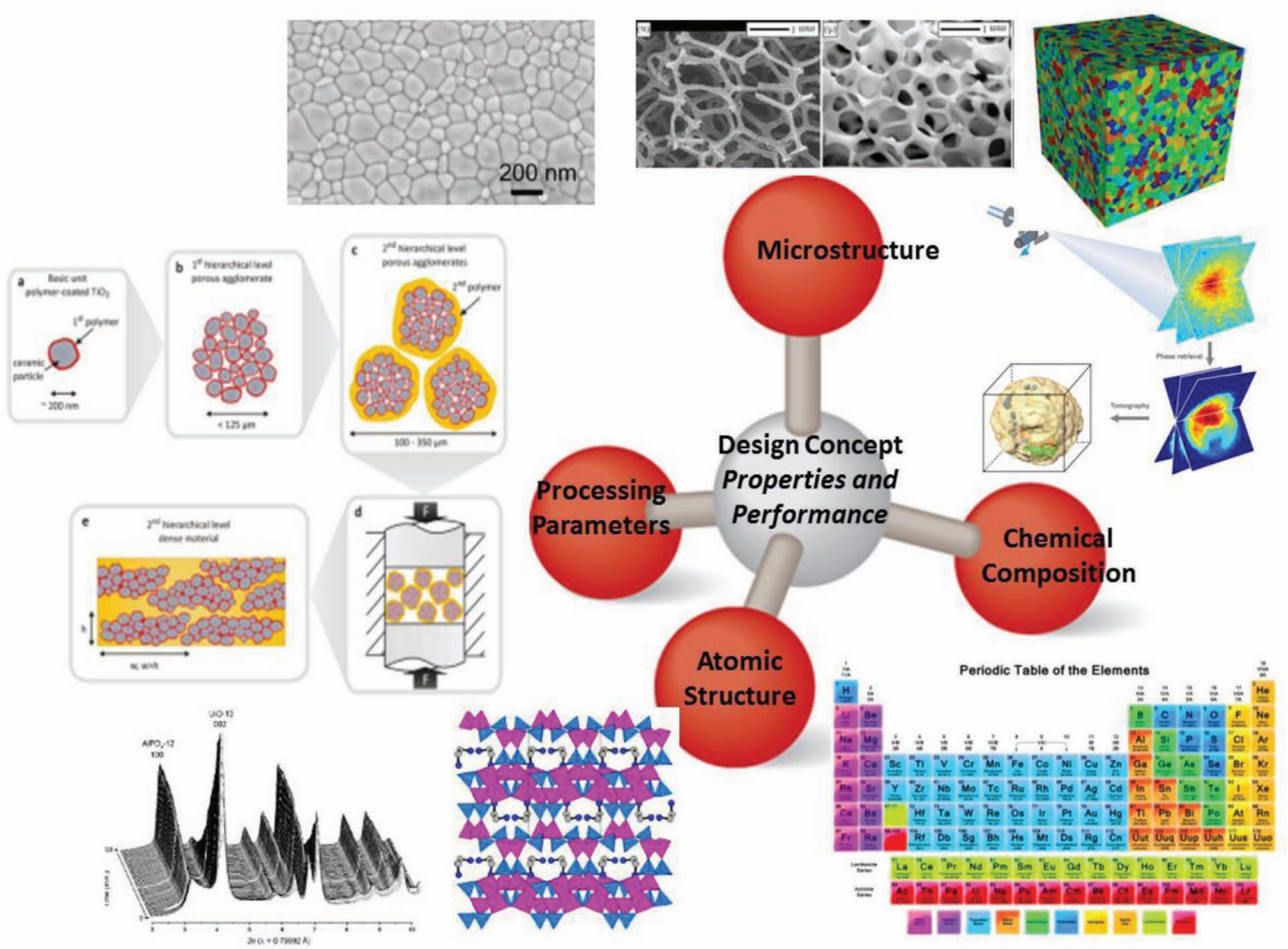

Fig. 1 : Illustration depicting the intimate tie of the chemical composition, atomic structure, processing parameters, and microstructure to the macroscopic properties of a material.

Colloidal materials can be applied by inkjet printing and electrophoretic deposition in the form of films, tapes, or screen-printing in layered approaches [5, 6]. Monolithic components are formed by methods including injection molding, gel casting [7], direct coagulation casting, tape-casting, and robocasting [8]. In addition, recent treatments of colloidal processing of ceramics relate to the novel manufacturing needs of direct deposition in advanced manufacturing or in porous material fabrication [9–13]. In these manufacturing processes, it is fundamental to create dispersions of particles in liquids, which is a research topic of several groups [1, 14, 15]. The primary advantage of colloidal ceramic processing is the minimization of microstructural flaws by creating well-mixed particle systems with uniform density [4, 11].

Many electronic components fabricated from oxide ceramics contain multiple cations either in the crystal structure or as dopants to alter electronic properties or microstructure. Applications of ceramics are based on the functional properties of electroceramics, and include varistor materials for surge protectors, oxygen and ion membranes in solid oxide fuel cells (SOFCs) [16, 17], charge storage in capacitors, piezoelectric actuators, catalysts [18, 19], oxygen membranes [20], gas sensor applications [21], and ongoing research for many other devices. These ceramic devices were made possible by vast improvements in the ability of experts to fabricate ceramic materials as powders with controlled composition, purity, size and shape, and thereafter form and consolidate components from these powders with high density and low flaw population [4, 22–26]. When properly combined with a forming technique, either near-net (slip casting, pressure casting, freeze casting, gelcasting, etc.) or bulk shape (dry pressing, isostatic pressing, etc.) and either pressureless or pressure-driven sintering, colloidal synthesis can produce dense, complex-shaped components with engineered microstructures. Control over the final microstructure of a sintered component requires an intimate connection between the initial materials and the processing pathway inherent in the manufacturing method.

New research challenges for ceramic material development include greater understanding of interfaces and phases in ceramics, prediction and control of heterogeneous microstructures, finer control over grain size during consolidation and densification, and control over the properties of oxide electronics [27]. When colloidal ceramics of multicomponent oxides are processed, their chemical stability begins to exhibit paramount importance, and has only become more critical as nanosized particle dispersions are utilized. Some ceramics like alumina or CoO develop surface hydration reactions that impact processing [28, 29]. The influence of the surface can strongly affect materi-

al properties, and has shown that the impact of surface hydration can alter phase stability for many nanoparticle systems [30–35]. Leaching of a component can be a deleterious phenomenon, and can create microstructural issues from component segregation and grain growth. For example, the Ce^{3+} or Y^{3+} in doped ZrO_2 milling media can be leached under acidic conditions [36, 37]. Perovskite ceramics structured as ABO_3 (A = divalent cations Ca, Ba, Pb, Sr; B = tetravalent cations Ti, Zr, Nb) experience these issues in acidic solutions as well. Lead magnesium niobate, $CaTiO_3$, $BaTiO_3$, and mixed $(Ca+Ba)(Ti+Zr)O_3$ perovskites all exhibit leaching of A site cations in acidic conditions [38–41]. Also, perovskites based on other cations such as Fe or Mn that exhibit multiple oxidation states can experience solubility changes due to oxidation or reduction reactions within the solution. Aluminum-doped ZnO exhibits environmental sensitivity, reacting with ambient humidity and CO_2 gas to form layered carbonate hydroxide hydrates, with loss of desired properties [42]. *A priori* predictions of cation stability can be difficult to provide based on the material system, and multicomponent ceramics having several dopants such as ZnO varistor ceramics with Bi, Mn, Co, and Al dopants must be screened for the best pH to minimize solubility [43].

The focus of this review is a practical approach to mitigating the problems noted in these multicomponent systems, while maintaining the advantages of the colloidal approach to ceramic processing. There are related processes in the five stages of colloidal processing between powder fabrication, dispersion, processing and consolidation that influence surface properties such as hydration reactions, component leaching, and microstructural development [1]. The chemistry for fabricating the desired colloidal phase is an indicator for methods to maintain the integrity of the powder during colloidal processing, and thereby provide the desired elemental distribution for sintering the component. By understanding how these effects are interrelated, the successful realization of advanced materials properties can be enabled by practitioners of the art.

II. Preparation of Metal Oxide Colloidal Powders

There are numerous approaches to synthesizing electronic ceramic powders, evolving considerably over approximately the past 70 years. There are several books discussing ceramic materials and more specifically electronic ceramics. We have found the books by Loehman and by Carter and Norton to be particularly helpful [44, 45]. Both books contain sections on ceramic powder synthesis and are a good starting point for a survey of different preparation methods. Our primary focus will be on the low-temperature-solution-based approaches such as sol-gel and chemical precipitation routes to synthesize these materials. However, there are other viable and mature methods of producing ceramic powders that should at the very least be covered briefly.

The very first syntheses of electronic ceramic powders were through solid state chemistry or what is often referred to as the mixed oxide route, which is still commonly used by manufacturers of metal oxide materials and devices today [46–48]. This process has fundamental shortcomings in that reacting species must diffuse distances up to 10^5 Å, which can make the formation of phase-pure materials challenging. Mechanical attrition or ball milling has proven capable of producing nanocrystalline powders but does require a starting material of the desired phase that must be acquired or produced by another means [49, 50]. Additionally, contamination from the milling media can be an issue. Milling can be a helpful processing step for reducing the size of mixed oxide reagents, increasing their homogeneity, and decreasing required diffusion distances. Furthermore, milling can be a helpful post-processing step in breaking up agglomerates and reducing the particle size of ceramics synthesized via solid-state reactions and any of the other techniques discussed below.

The flame synthesis of materials is capable of synthesizing mixed oxides, metals, and metal salts in nanoparticle form at high rates (up to 1 kg/h at the research laboratory scale). Strobel and Pratsinis put together an excellent review of flame-made smart nanostructured materials and do a good job of reviewing existing flame synthesis papers and previous review articles [51]. The broader field of combustion synthesis, which includes flame synthesis, is covered in a review article written by Patil, Aruna, and Mimani [52]. This particular review focuses on solid-state combustion (SSC) and solution combustion (SC) in addition to pointing the reader toward articles reviewing other combustion synthesis approaches in greater depth.

(1) Chemical solution synthesis routes

Many solution-based syntheses have been developed over the years for the preparation of electronic ceramic powders. Quite often, solution-based preparations for ceramic powders have higher purity and lower flaw populations, but can exhibit reactivity at lower temperature. However, if controlled properly, the higher reactivity combined with a high surface area can lead to more efficient densification into bulk materials. One route that can begin with any number of starting solutions and suspensions including aqueous, organic, and even supercritical CO_2 solutions and produce porous and nanostructured materials is controlled freezing and freeze drying [53]. Sol-gel processing as a route to form ceramic powders and solution-based chemical precipitation will be discussed in more detail later and will be a large focus in this section of the review. However, it would be inappropriate to not first cover solvothermal and hydrothermal synthesis of ceramics and direct the reader to some selected publications and excellent review articles.

Hydrothermal preparations have been quite effective at producing a wide variety of phases, shapes, and sizes of electronic ceramics, particularly the perovskite materials. Commercial hydrothermal syntheses involve water at pressures ranging between approximately 1 and 1000 bar and temperature of 100–300 °C [54]. Hydrothermal reactions can proceed under autogenous pressure, P, related to the operating temperature, degree of fill, and stirring, but also include more exotic approaches which include hydrothermal electrochemical, sonochemical, and microwave syntheses [54]. The research community as whole has been exceptionally prolific in developing and publishing hydrothermal routes to produce perovskite and

other ceramics, beginning with a patent issued in 1940 for the synthesis of alkaline earth metal titanates [55]. The amount of literature available on hydrothermal preparations of barium titanate alone is almost overwhelming and includes syntheses that produce spherical or cube-like particles with rounded corners but also rods and more exotic shapes that resemble starfish and swords [55–58].

When you broaden the field slightly to include solvothermal routes (where non-aqueous solvents are used in a relatively similar manner to produce ceramic materials), the amount of published literature expands even more. Once again, barium titanate serves as an almost model system and a number of different solvothermal preparations have been published [59–61]. The review on the solvothermal synthesis of perovskites and pyrochlores written by Modeshia and Walton is particularly insightful [62]. Although the focus of the Modeshia and Walton 2010 review is solvothermal syntheses, they summarize a fair amount of the literature available on the hydrothermal synthesis of pyrochlores and perovskites, and even go as far as saying that aqueous solvents may still be required for the synthesis of materials where high alkalinity is necessary to achieve sufficient concentrations of hydroxide precursors. When the precursors can be sufficiently solubilized, Modeshia and Walton argue that in addition to several other benefits, solvothermal synthesis offers a route to complex, multi-element materials with hierarchical order and the production of novel compositions of materials not previously possible through conventional routes.

Although the scientific community has been quite successful at developing hydrothermal and solvothermal preparations of ceramic materials with fine control over phase, size, shape, and porosity there remains a large gap in our understanding of the details of most solution-based crystal growth. Lencka and Riman have made some significant inroads into our understanding of the optimal conditions for solvation and crystal growth through their careful study of hydrothermal syntheses. They first proposed a rigorous thermodynamic model for the hydrothermal prep of barium and lead titanates, developing phase stability diagrams for the reagents and intermediates present during perovskite formation [63, 64].Their work progressed to include other perovskites such as calcium titanate, strontium zirconate, PZT, and sodium and potassium bismuth titanates [65–68]. The Lencka-Riman thermodynamic model is gaining broader recognition and is being applied by other chemists. In fact, a group at Huazhong University of Science and Technology used the Lencka-Riman model to design and optimize synthesis for $KNbO_3$ and carry out powder preparation [69].

Many electronic applications require dopant populations that are non-stoichiometric or non-equilibrium phases, and rigorous thermodynamic models for their synthesis and the stability of their precursors in solution are not yet attainable. In many of these cases, sol-gel or chemical precipitation routes allow for better compositional control. Sol-gel science originally focused on the synthesis of monolithic ceramics and glasses, films, and fibers but the understanding developed in processing these materials was instrumental in developing sol-gel routes for powder synthesis. The literature available on sol-gel science is enormous and a complete review is not possible here. In 1987, Roy published a solid review of sol-gel science used in the production of ceramics [70]. Messing and Minehan have an extensive publication record in this field and their 1991 review describes the development of sol-gel science and its application to powder synthesis [71]. Most of the early sol-gel routes (and still a significant percentage of the newer approaches as well) to produce ceramic powders used metal alkoxides as reagents. Mazdiyasni pioneered the alkoxide sol-gel path to ceramic powders during the 1960s and 1970s and applied this method to fabricate a broad set of materials [72].

Over time, modifications were made to the alkoxide based sol-gel route to synthesize an increasingly broad set of materials. For example, the stearic acid sol-gel route yielded high-purity homogeneous nanopowders at a low processing temperature [73–75]. Other researchers developed sol-gel syntheses that used acetylacetonate precursors and included poly(vinyl alcohol), or PVA, and still another approach used metal nitrate reagents combined with citric acid and glycol [76, 77]. A related route to produce ceramic powders is the precipitation or coprecipitation synthesis method. In a coprecipitation synthesis, reagents are stabilized in solution (often under acidic conditions) and are then simultaneously precipitated (quite often through a rapid increase in pH) to produce an amorphous and homogeneous powder of carbonates, citrates, or hydroxides [78–81]. In some cases, the distinction between sol-gel and chemical precipitation routes can become blurred, particularly in more modern approaches where ceramic nanoparticles are nucleated and grown in solution and sometimes through the careful use of stabilizing ligands, remain suspended in colloidal solution for extended periods [82–87].

As with other synthesis approaches, sol-gel routes are sensitive to reagent and processing choices, which affect hydrolysis rates and impact particle properties such as shape and size, and state of aggregation. Both TiO_2 and $BaTiO_3$ can be formed readily, but the solvent and reactant decisions can lead to varying products. In 2002, Oskam and coworkers used a modified sol-gel preparation in water for titania synthesis, with nitric acid as a catalyst [88]. The reaction proceeds via the two-step hydrolysis of titanium isopropoxide and subsequent condensation of the hydrolysis products with a high yield of TiO_2 particles. However, these particles demonstrate both irregular shape and agglomeration, as can be seen in a TEM image of particles in Fig. 2a. Use of isopropanol as both a solvent and a ligand slowed the reaction rate between water and titanium isopropoxide, by allowing for ligand exchange and the formation of clusters of primary alkoxides and titanium [84]. This results in TiO_2 nanoparticles with improved shape and a narrow size distribution (diameters of 4.4 ± 1.8 nm) as can be seen in Fig. 2b.

For a number of decades, quite a number of research groups synthesized barium titanate powders by simultaneously hydrolyzing barium and titanium alkoxides, which is summarized via the reaction below [47, 89, 90].

$$Ti(OR)_4 + Ba(OH)_2 \rightleftharpoons BaTiO_3 \quad (1)$$

Small modifications to the titania sol-gel prep discussed above, including the addition of barium hydroxide as a reagent, can be used to synthesize crystalline barium titanate nanoparticles of approximately 10 nm in diameter at a modest temperature of 80 °C. By using isopropanol as a solvent and slowly adding water to the reaction (in a very similar fashion to the TiO_2 nanoparticle synthesis), the Baik research group was able to slow the alkoxide-hydroxide hydrolysis and condensation sufficiently to form nanoparticles [86, 91]. The amount of water added during the hydrolysis step can move the stable crystalline phase of the synthesized particles from tetragonal to cubic [86]. After including air-free chemistry preparatory and synthesis techniques and applying more precise control over the amount of water during the nanoparticle synthesis, a $Ba(OH)_2{\times}8H_2O{:}H_2O$ molar ratio of 1:60 was determined as optimal for driving the reaction to completion while obtaining the largest difference between the c and a-axis lengths. A TEM image of $BaTiO_3$ nanoparticles synthesized using this $Ba(OH)_2{\times}8H_2O{:}H_2O$ ratio is shown in Fig. 2c. Sandia researchers have also demonstrated that by partial substitution of the barium hydroxide octahydrate with strontium hydroxide, nanoparticles of the solid-solution $Ba_xSr_{1-x}TiO_3$ (BST) can be synthesized with no other modifications. The same synthesis can be performed with very similar results (except for a noticeable change in particle dispersion and solution stability) using ethanol rather than isopropanol. By changing the alcohol, the surfactant bound to the barium titanate nanoparticle surface would also change since the alcohol acts as both a solvent and a ligand. The change in dispersion of the particles is readily apparent in the TEM of the $BaTiO_3$ nanoparticles synthesized in ethanol (see Fig. 2d and compare to Fig. 2c).

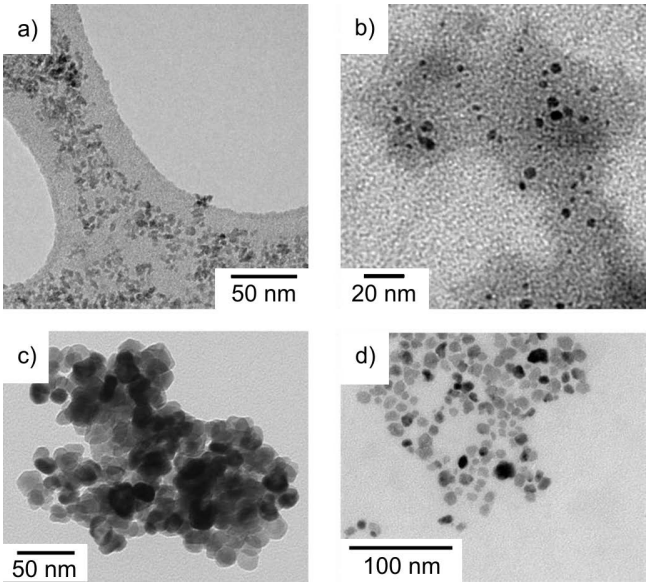

Fig. 2: TEM comparison of processing routes for TiO_2 and $BaTiO_3$ nanoparticles.

(2) Chemical precipitation of ceramics

The chemical preparation of ceramics developed out of the need for large-volume sources of high-purity materials. High-temperature calcination of powder mixtures of carbonates and oxides to produce ceramic powders result in grain growth and porous particle production, with a resulting need to mill powders to a lower particle size for component pressing or colloidal processing. These methods tend to be energy-intensive, and as mentioned previously, impart impurities from the media used in the milling operations, often having a deleterious effect on electronic properties. Chemical precipitation or co-precipitation routes also offer opportunities to exert control over particle size, shape and distribution of elements by successive coating reactions to form core-shell topologies, and in some cases lead directly to dispersions for the next stage in powder preparation.

As discussed in the previous section, chemical precipitation strategies tend to operate with the goal of creating elemental mixtures on the atomic level in solutions, followed by rapid precipitation of a compound precursor by addition of the desired reactant [22–25]. A specific example is the oxalate precipitation route, in which metal cations are uniformly dissolved in acidic conditions in the first solution, while a reactant solution of oxalic acid is used as the precipitant [92–102] Precipitation is based on the solubility product reaction (as written for divalent cations):

$$MC_2CO_4 \rightleftharpoons M^{2+} + C_2O_4^{2-}(aq)$$
$$K_{sp} = \frac{[M^{2+}][C_2O_4^{2-}(aq)]}{[MC_2CO_4]} \quad (2)$$

A homogeneous supersaturated solution of desired metal cations for the final oxide can be prepared in acidic media using chloride or nitrate precursor salts, and precipitation initiated by rapidly adding a second solution of oxalic acid under high shear conditions. Rapid mixing of the two solutions leads to precipitation of a mixed metal oxalate, which can be calcined into a uniform oxide powder at temperatures low enough to avoid grain growth or sintering. Table 1 presents available values of the solubility product for several oxalate compounds, and in many cases, the solubility product K_{sp} of the reaction is very low. This means mixed cations in homogeneous solution will rapidly react with oxalate ions to form solid particles. There are exceptions, such as magnesium or thallium, and other elements such as silicon and vanadium, that do not form insoluble oxalate compounds. These materials are more suitable for production via sol-gel chemistry or other chemical routes. Nevertheless, oxalate precipitation is a highly flexible and efficient route to large-scale ceramic production.

Solution chemistry must still be considered in these procedures, and care given to the precursor materials and use of additives. Therefore, pH effects can impact the precipitate phase during the reaction, and affect size or shape properties. In addition, the cation hydrolysis reactions are also affected by pH, and affect the speciation and hydroxide solubility limit of the materials. For this reason, nonaqueous solvents are also used with the oxalate co-precipitation route [103–105]. More detailed description of any particular cation hydrolysis reaction can be found in Baes and Mesmer [106].

Table 1: Solubility product for metal oxalates in water.

Name	**Formula**	**pK_a**	**K_{sp}**
Barium Oxalate	BaC_2O_4	6.79	1.6×10^{-7}
Calcium Oxalate Hydrate	$CaC_2O_4.H_2O$	8.63	2.32×10^{-9}
Cerium Oxalate Nonahydrate	$Ce_2(C_2O_4)_3 \cdot 9H_2O$	25.50	3.2×10^{-26}
Copper Oxalate	CuC_2O_4	9.35	4.43×10^{-10}
Gold (III) Oxalate	$Au_2(C_2O_4)_3$	10	1×10^{-10}
Iron Oxalate Dihydrate	$FeC_2O_4 \cdot 2H_2O$	6.5	3.2×10^{-7}
Lanthanum Oxalate Nonahydrate	$La_2(C_2O_4)_3 \cdot 9H_2O$	26.60	2.5×10^{-27}
Lead Oxalate	$Pb\ C_2O_4$	9.32	4.8×10^{-10}
Magnesium Oxalate Dihydrate	$MgC_2O_4 \cdot 2H_2O$	5.32	4.83×10^{-6}
Manganese Oxalate Dihydrate	$MnC_2O_4 \cdot 2H_2O$	6.77	1.70×10^{-7}
Mercury (I) Oxalate	$Hg_2\ C_2O_4$	12.76	1.75×10^{-13}
Nickel Oxalate	NiC_2O_4	9.4	4×10^{-10}
Silver Oxalate	$Ag_2C_2O_4$	11.27	5.40×10^{-12}
Strontium Oxalate Hydrate	$SrC_2O_4\ H_2O$	6.80	1.6×10^{-7}
Thallium (I) Oxalate	$Tl_2C_2O_4$	3.7	2×10^{-4}
Thorium Oxalate	$Th(C_2O_4)_2$	22	1×10^{-22}
Yttrium Oxalate	$Y_2(C_2O_4)_3$	28.28	5.3×10^{-29}
Zinc Oxalate Dihydrate	$ZnC_2O_4 \cdot 2H_20$	8.86	1.38×10^{-9}

For example, the non-ohmic ZnO-based ceramics have been widely used as varistors for voltage stabilization and transient surge suppression in electronic circuits and electric power systems since the late 1960s. This type of varistor is a ceramic semiconductor based on zinc oxide, ZnO, and various dopant elements resulting in a component having a highly nonlinear current-voltage relationship [107, 108]. The varistors typically contained > 98.4 mol% of zinc oxide with the additives of bismuth oxide along with oxides of cobalt and/or manganese. Synthesis of the powder was a three-stage process, with the first stage generating Co-Mn-Al doped zincite powder. Aqueous chloride salts of Zn, Co, Mn, and Al are combined and diluted to a specified volume. A hydrous oxide co-precipitate is formed by means of the rapid addition of a concentrated aqueous NaOH solution. After two minutes, a saturated, aqueous solution of oxalic acid (heated to ~ 50 °C) is added to convert the co-precipitate to its corresponding metal oxalates. The slurry is continuously stirred until the pH reaches 8.0, at which time it is pumped into filter funnels, washed with deionized water, and then acetone. The dried cake is calcined at 600 °C to convert the oxalates to oxides. For stage two, a bismuth nitrate solution is added to an aqueous slurry of the zincite powder, mixed for a short period of time, filtered, washed, and then calcined to convert the bismuth nitrate to bismuth oxide. The final stage involves the addition of a sodium oxalate solution to an aqueous slurry of the Bi-doped zincite powder. The resulting slurry is freeze-dried to prevent segregation of the Na, and then calcined to generate the final powder. Fig. 3 provides a high-level flow chart of the synthesis procedure. The SEM images, shown in Fig. 4, provide the approximate particle size and morphology of the final ZnO-based varistor powder as synthesized following this process.

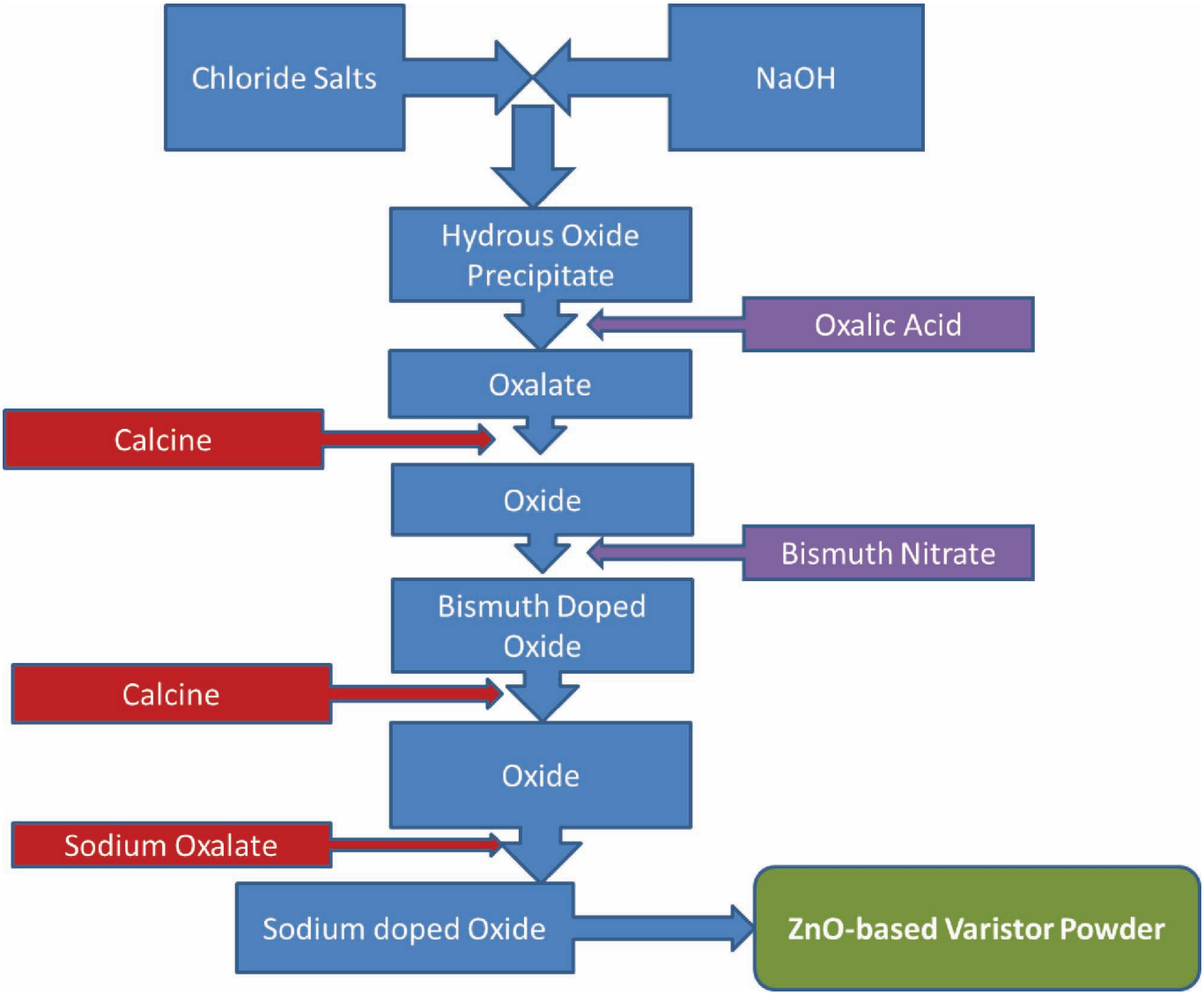

Fig. 3 : High-level flow chart of the synthesis process for chemically prepared ZnO-based varistor powder.

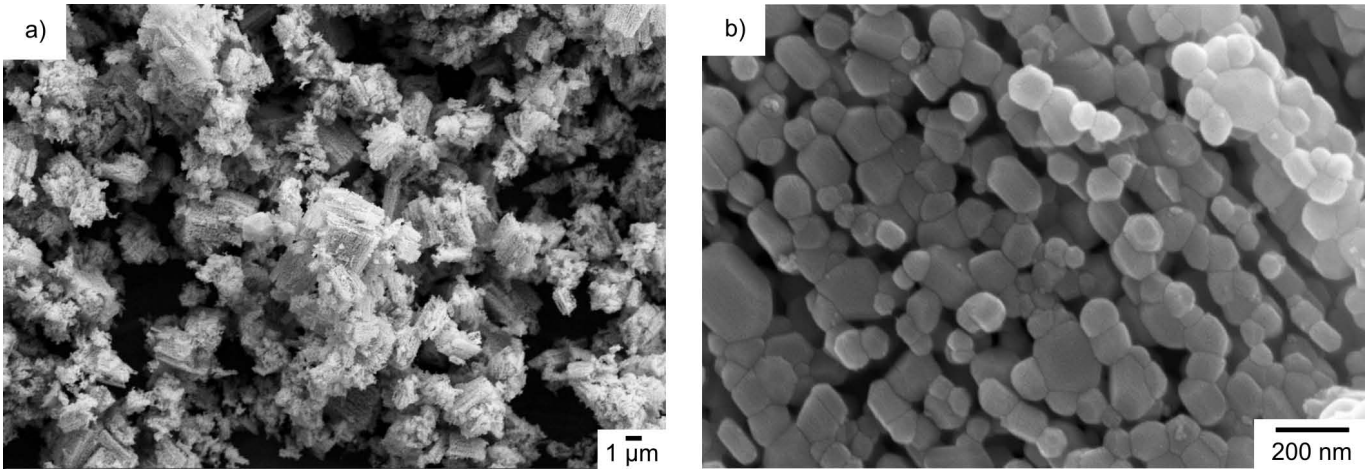

Fig. 4 : SEM images of the final chemical precipitated ZnO-based varistor powder.

III. Milling Processes

Milling operations are required for many powders produced by chemical precipitation routes such as oxalate coprecipitation, sol-gel powder synthesis followed by calcination, flame combustion synthesis, and the traditional mixed oxide preparation. For manufactured powders prepared with a calcination or conversion reaction, there is often the formation of soft or hard agglomerates. This leads to the need to break down these larger solids into fine particle dispersions by energetic milling operations. These techniques are common over virtually all powder processing industries, ranging among mineral recovery, ceramic

materials, paper production, and pharmaceuticals. Methods for breaking down particles into smaller and more uniform size distributions are highly energy intensive, and can consume up to 70 % of the power requirements of mineral recovery techniques [109].

Wet milling is energetically more favorable, and can be promoted by the control of the solution pH to generate surface charge, or by the addition of dispersants [110–113]. Agglomerate breakup leads to significantly higher number concentration of particles, and without an effective barrier to agglomeration, coagulation is rapid [114]. Conditions for colloidal stability are needed to prevent reagglomeration and allow for greater shear and grinding interactions to lower particle size. The variation or choice of solvent and pH is a critical factor in material stability. Chemically aggressive or corrosive conditions can lead to solubility of the chemical species from the ceramic. Such processes impact microstructural development during consolidation reactions and are best avoided.

There are two processes active in media milling. *Deagglomeration* is the process of breaking up particles in physical contact, but without strong chemical bonds or necessarily having grain boundaries. Single crystals are not broken in the deagglomeration stage. *Comminution* processes are methods that fracture particles based on three mechanisms:

(1) Abrasion occurs when particles experience shear forces between rotating and moving media. Fine fragments are produced from the parent particle.
(2) Cleavage of a parent particle occurs from compressive forces, generally operating from slower rates of impact. The resulting particles generally are of the same particle size, as a fraction of the initial material.
(3) Fracture results from rapid, intense stresses and can form daughter particles 20 – 70 % of the parent particle size.

Coarse particles are milled based on cleavage and fracture mechanisms, whereas finer particles experience cleavage and abrasion by compressive forces and shear in a packed bed [115]. Particle fracture leads to the introduction of new surface to the solution phase, and reaction with water by hydration or leaching can produce changes in pH, or require additional dispersant. The reduction of particle size by comminution involves the exposure of new surface area with each fracture or cleavage event. Table 2 compiles experimental values for surface energy of many oxides, both in the hydrated and non-hydrated states. The energy input to the milling process is believed to be related to this new surface energy, while admittedly highly efficient processes are far from obtainable.

Table 2: Interfacial properties of known electronic ceramics.

Material	Surface Energy (J/m^2) [31, 34, 182, 269 – 273]		Hamaker Constant (x10^{-20} J) by Lifshitz Theory				Isoelectric Point (IEP) [139 – 142, 274, 275]
	Hydrous	Anhydrous	A_{131} (Water)	A_{131} (Toluene)	A_{131} (Ethanol)	A_{131} (Ethylene Glycol)	
$BaTiO_3$ (average)	3.69 ± 0.22	3.99 ± 0.28	8.0	8.20	10.1	4.44	5 – 6,6.5 [276]
$CaTiO_3$	2.49 ± 0.12	2.79 ±0.13	N/A	N/A	N/A	N/A	3 – 4, 8.1 [176]
$PbTiO_3$	1.97 ± 0.67	1.11 ± 0.23	N/A	N/A	N/A	N/A	5 – 7 [178]
$SrTiO_3$	2.55 ± 0.15	2.85 ± 0.15	4.77	4.47	5.06	2.72	N/A
SiO_2	~ 1	~ 0.6	0.46	0.203	5.17	3.14	< 3
TiO_2	1.29 ± 0.08	2.22 ± 0.07	5.35	5.01	5.58	2.64	5.1 – 6.4
Al_2O_3	0.4	2.0	3.67	4.93	4.17	5.14	6 – 9.9
Fe_3O_4 (Magnetite)	0.80 ± 0.05	N/A	3.3	0.9	1.53	2.39	6.5 – 6.9 [277]
γ-Fe_2O_3 (Maghemite)	0.58 ± 0.2	0.6 ± 0.2	3.6	1.8	1.98	1.26	6.6
α-Fe_2O_3 (Hematite)	0.75 ± 0.16	N/A	3.9	2.9	2.60	1.29	7.6 – 8.6
CeO_2	0.86 ± 0.02	1.16 ± 0.02	4.1	2.62	3.06	1.48	8.1 – 8.4
ZnO	1.31 ± 0.23	2.55 ± 0.07	1.89	1.291	1.70	1.76	8.6 – 9.2
ZrO_2 (tetr.)	1.02 ± 0.05	1.23 ± 0.04	7.23	N/A	N/A	N/A	4 – 6
3Y or 8Y-ZrO_2	1.02 ± 0.05	1.32 ± 0.06	7.23	7.42	7.72	6.06	7

Stirred media mills can apply greater power and energy to the milling process [28, 116, 117]. An attritor mill combines forces of impact, abrasion, and shear during the energetic collision, flow, and rotation of media and the stirring arms and between particles. The stirring arms generate (1) impact forces between media, (2) rotational forces on the media, and (3) tumbling forces as mixing occurs. Particles are sheared between grinding surfaces of the media from these multiple motions. Fracture occurs owing to both compressive and shearing stresses [118]. This results in much shorter times for comminution than ball or vibratory milling.

Kwade described the efficiency of the comminution process as based on the number of stress events and the intensity acting at these stress events [119]. The number of stress events is related to the loading of particles, and grinding efficiency is noted to increase with the solids loading. The grinding events will relate to the surface area of the media, and by extension the media size. The intensity at the stress event is proportional to the stress energy at the event. This factor is related to the velocity of the media during motion, which is maximized at the tip of the stirring arms. This leads to *stress energy* (SE) being defined as a function of the kinetic energy of agitated grinding media with density ϱ_{GM} and size d_{GM} at the tip speed velocity, v.[120–123]

$$SE_{gm} = d_{gm}^3 \rho_{GM} v v_{GM}^2 \quad (3)$$

This definition allows for relating the effect of media size and the tip speed of the mill to the development of finer particle sizes. The product of the stress event and intensity was reasoned as a good measure of the overall energy consumption of the mill process. As a result, the specific energy of the mill is a parameter that can be followed for determining the milling process.

The *specific energy input* (SEI) during milling is calculated via the expression:

$$E_{m,V} = \frac{\int_0^\tau (N(\tau)-N_0)d\tau}{m_p - 0.5\triangle m_{GM}} \text{ in kJ/kg} \quad (4)$$

The mass of the solid product is m_p, the power at times 0 and time τ is given by N_0 and $N(\tau)$, and the wear of the grinding media relates to the power input N. Media wear is an issue in high-energy milling, and values from 2 to 10 % have been reported based on the intensity of the milling procedure [117, 118, 124]. Specific energy is proportional to the product of the total number of stress events, the stress number SN, and the stress energy SE, the energy transferred to a product particle. Stenger showed that identical comminution results are obtained if two of the three parameters – specific energy, number of stress events, and stress energy – are equal [117].

(3) Chemically aided milling

Aqueous processing is driven by environmental concerns, and as a result the role of interfacial reactions on particle surfaces in water is more prominent. The development of high particle concentration, surface reactions that deleteriously impact dispersion stability, shear-induced agglomeration, gelation, or aging can all prevent application of the dispersion to manufacturing operations. The need to maintain material stability under the energetic milling operations has led to consideration of the chemical stability of particle interfaces [125]. Strategies that consider surface reactions are employed to prevent dopant or component leaching, and suppress the formation of new phases. Chemically aided milling is an attempt to prevent surface reactions while inducing colloidal stability in a dynamically milled system, and is also termed the "passivation-dispersion" approach [125]. Chemically aided milling considers two problems in slip preparation: (a) surface passivation to prevent solubilization of species during milling, and (b) control over solution conditions such as pH and dispersant concentration.

A passivating agent is any solution additive that promotes surface or interfacial stability, and is thus either a surface-active agent or forms surface-precipitate layers. It can have the additional synergistic effects of increasing surface potential, promoting efficient wetting, lowering solubility at the desired pH, or promote the adsorption of a stabilizing surfactant. This passivation-dispersion approach should minimize energy and time to produce stable, high-solids loading aqueous dispersions of electronic ceramics. Many water soluble ions can be passivated with sparingly soluble salts, similarly to the oxalate process for preparing the mixed oxide powder. In practice, the formation of new surface phases as particle surface area is increased requires the dynamic monitoring of the milled solution and the addition of surface passivants and dispersing agents during the process. For any specific surface area, there are optimal concentrations of passivant and dispersant. The solution is monitored to correct for changes in pH, conductivity, or dispersant concentration to maintain optimal conditions for dispersion and interfacial stability. Excess passivant can lead to the formation of secondary phases. Clearly, the strategies of chemical preparation methods such as the oxalate co-precipitation route align with the concept for oxalate ion use in chemically aided milling.

IV. Interaction Energy Calculations in Colloidal Processing

The second component of practical processing of multication ceramics is the dispersion stability of the multication oxide particles. In colloidal theory, there are many textbooks and reviews for the generation of dispersed systems and control over rheological properties [126]. The principles of colloidal stabilization are based on the summation of the interactions between particles, and the generation of an interaction energy diagram between two ideal particles. These consist of the ubiquitous Van der Waals attraction, and any repulsive forces based on surface potential and/or the adsorption of polymer layers (uncharged or charged). Free or unadsorbed polymers can lead to either attractive or repulsive interactions as depletion interactions, and details are given in other reviews [14].

(1) Van der Waals attraction

For identical particles (composition and crystal structure) in a fluid, there will always be an attractive interaction related to the electronic dipole interactions of the atomic structure of the system. This incorporates the permanent and induced dipolar interactions (London, van der

Waals, and dispersion forces) related to the polarization of the electron cloud of one atom with another. These properties of the materials can be summarized into a single term known as the Hamaker constant A_H[127], which is used for relating the attractive forces between identical particles of radius *R* with the following equation [126].

$$V_{vdW}(H) = -\frac{A_H R}{6H} \quad (5)$$

where surface-to-surface distance is represented by H. This expression does not account for retardation or screening effects, which reduce van der Waals attraction more rapidly than the expression accounts for, and details can be found in Isrealachvili for corrections [127]. This expression serves under the conditions that separations distances are close, less than 10 nm.

The Hamaker constant serves as a proxy for the propensity of the particles to aggregate, and a high value for the Hamaker constant suggests that particles will flocculate rapidly to form fractal aggregates, whereas small values of A_H are expected to trend toward facile dispersion, and sedimentation into high-packing-density compacts. There are several reviews of the calculation of Hamaker constants from varying types of measurements, including optical constants and surface wetting measurements [128–136]. Table 2 presents a collection of the calculated Hamaker constants for several typical electronic ceramics used in the fields of dielectric materials, solid oxide fuel cells, and opto-electronic ceramics. The values presented assume the powder is present in the listed fluid phase. Not all materials have available parameters for calculation at present.

The van der Waals interaction forces are inversely related to the separation distance as 1/H, and in any case show that a repulsive interaction is needed to create a stable colloidal system. The depth of the attractive force is generally related to the thermal energy of the system, and separation of particles to a level of 1 – 2 kT is often taken as suitable for a well-dispersed system to be developed. However, often the solids loading desired in the system requires particles to avoid attraction at very close distances. The summation of interaction forces leads to a varying profile between particles, and can create optimal separation distances δ, in which particles have low or zero interaction energy, thereby approximating a system in which particles behave as "hard spheres".

The separation distance establishing this control over macroscopic rheology impacts the effective volume fraction of the particles, ϕ_{eff}, expressed as follows.

$$\phi_{eff} = \phi\left(1+\frac{\delta}{r}\right)^3 \quad (6)$$

The effective volume fraction becomes most significant in the dispersion of nanoparticle systems, in which the dispersion distance can be an appreciable fraction of the particle separation distance. Kamiuya and Iijima provide greater discussion of this point for the interested reader [137].

V. Surface Chemistry and Aqueous Stability of Multicomponent Ceramics

Metal oxides can be characterized by the pH at which surface charge is negligible, known electrokinetically as the "isoelectric point" or IEP, or as variations in the "point of zero charge", which has three conventions: the point of zero net proton charge (PZNPC), the point of zero net charge (PZNC) where intrinsic surface charge is zero, and the PZC, where the net total particle charge is zero [138]. The PZC or isoelectric point of the powder is commonly avoided in milling, as undispersed materials would prevent the grinding operations. Kosmulski has compiled and evaluated data on the point of zero charge (PZC) for metal oxides, with average values given in Table 1 [139–142]. A solution pH far from this value will either generate positive charge in acidic conditions, or negative charge in basic conditions, sufficient to create electrostatic repulsion. The PZC or the IEP of a solid (and its charging mechanism in solution) will play a strong role in the adsorption mechanism of any surfactant, and in any competition for the surface with other components of the dispersion.

It is relevant therefore to determine charging behavior or the variation in zeta potential with pH for any dispersion strategy to be successful. Trends in PZC related to ion valence were also compiled by Kosmulski [139], showing a rough correlation between valence and PZC. In general, low-valence oxides have more basic or neutral PZC, and the PZC becomes more acidic as valence increases. However, there is still a wide range reported for metal oxides with valence of 4, having PZC values ranging from 2 to 9. Usually the PZC of mixed oxides changes linearly from the PZC of one component to the other. As an example, perovskite oxides can develop either acidic or basic surface properties based on composition and reaction with surface water [143, 144].

The stability of a nanoparticle suspension is affected by many surface-solution interactions [145], but a sufficiently high surface or zeta potential would conceivably stabilize a nanoparticle dispersion by electrostatics alone. Achieving the maximum value of the zeta potential for nanoparticles would be an obvious goal for creating stable systems. Yet, charge development and electrostatic surface potential for nanoparticle systems remain a topic of conflicting discussion. Liu, Chen and Su stated that TiO_2 nanoparticle stability was influenced by the presence of impurities, more so than the particle size or crystal phase [146]. Fazio *et al.* tested commercial and aerogel-produced TiO_2 nanoparticles, finding point of zero charge values roughly in line with published values [147]. Wang *et al.* claimed that metal oxide nanoparticles could shift their IEP by as much as 3 pH units as solids loading is increased [148]. Their explanation is that dissolved CO_2 forms bicarbonate ions, affecting the surface charge for low loadings of nanoparticles. Bulk behavior is found when solids content is raised. Yet, Jailani *et al.* examined the effect of nanoparticle size and solids loading upon zeta potential of alumina particles, and determined that the increased surface area of the powder resulted in greater electrolyte levels, leading to lower zeta potential values based on electrostatic screening [149]. Nanoparticles exhibit greater complexity in their surface charging behavior, which requires careful consideration of the model used to interpret measured data.

The electric double layer (EDL) arises from the interaction of thermal forces and the presence of an electric charge

at an interface. A charged surface (or particle) in an electrolyte solution forms a diffuse layer of ions, and a condensed layer of counterions at the surface. The condensed layer lowers the surface charge of the interface by screening charge and creates a measurable electrical capacitance. The diffuse layer of ions is created by the thermal motion of non-adsorbed ions in the electrolyte. The Gouy-Chapman model was developed for planar interfaces, whereas the Debye-Huckel model applies to spherical particles. Both models assume that the fluid phase is a continuum, and that ions are a continuous charge distribution [150].

Determining the electrostatic repulsion between charged surfaces requires solving the Poisson equation, using the Boltzmann equation for local ion density. This is a second order differential equation and a complete solution requires numerical calculations. The solution can be linearized, for specific cases. The nonlinear Poisson-Boltzmann equation is solved with an analytic expression for low potentials by assuming that ions are point charges interacting with a homogeneously charged interface. The point charge assumption is noted to fail for conditions of high surface charge density, which predicts too high a concentration of counterions at the surface. The volume of the counterions need to be considered in determining the more accurate structure of the interface.

Electrostatic repulsion between particles is common in water and alcohols due to the charging behavior of surface hydroxyl groups, generally present in any ceramic system. For identical particles of size R having the same constant surface potential ψ, the electrostatic repulsion has the form for separation distances H of:[127]

$$V_{ES}(H) = \frac{64\pi kTR\rho_{\infty}\psi^2}{\kappa^2}\exp(-\kappa H) \qquad (7)$$

The parameters for the expression include the Boltzmann constant, k, the absolute temperature T, the gas constant R, the surface (zeta) potential ψ, and the number density of ions in solution ρ_{∞}. The diffuse dielectric double layer has a distance solely affected by the ions in solution, known as the Debye length as $1/\kappa$. κ is calculated from the ionic concentrations, N_i, and valence, z_i, of each counterion of type *i* in the system as:

$$\frac{1}{\kappa} = \sqrt{\frac{e^2}{\varepsilon_r\varepsilon_0 kT}N_i Z_i^2} \qquad (8)$$

The components of this relationship include the electron charge e, the permittivity of free space ε_0, and the solvent dielectric constant ε_r. The thickness of these layers can be estimated by the product of particle size, *a*, and the Debye constant, κ, as the term κa. A "thin" double layer has a large value of κa ($\kappa a >> 1$), whereas a "thick" double layer has a small value of κa. For many treatments, it is common to assume a thin double layer in equilibrium with the surrounding electrolyte. However, this assumption can prove insufficient for cases where surface conductivity plays a role in the determination of the true zeta potential [151].

This expression for ionic strength highlights the effect of divalent or higher valency ion solubility to the electrostatic stability of a system. The squared power to the valence term can collapse electrostatic repulsion at low ion concentrations, leading to a lack of stability by electrostatic forces alone. Discussion in Israelachvili details the impact of divalent and trivalent ions in solution and their effect on interaction forces and colloidal stability, also known as the Schultz-Hardy rule (see also Morrison and Ross) [127, 152].

The electrical potential at interfaces can be measured by means of multiple techniques, including microelectrophoresis, electroosmosis, streaming potential [150], electrokinetic sonic amplitude [153] or colloid vibration current [154–156] A very common method for zeta potential measurement of colloids is electrophoresis, in which particle motion in an applied electric field is detected using light scattering techniques. The value of the particle zeta potential from electrophoretic mobility measurements is used to approximate the repulsive force from surface charge [157]. The zeta potential is extracted from the electrophoretic mobility, u_E, using Henry's equation [158].

$$u_E = \frac{2\varepsilon_0\varepsilon_r\zeta f(\kappa a)}{3\eta} \qquad (9)$$

In this expression, ζ is zeta potential, η is the solvent viscosity, ε_0 and ε_r are the permittivity of free space and the dielectric constant, and $f(\kappa a)$ is the Henry function, which varies smoothly from 1 to 1.5 as κa varies from 0 to infinity. The Henry function can be exactly calculated with numerical methods [159], but Ohshima developed analytical expressions that are highly accurate [160, 161]. For $\kappa a = 0$ (infinitely thick double layer) the Huckel approximation gives $f(\kappa a) = 1$. For low values of κa (infinitely thin double layer), the Smouchkowski approximation is assumed and $f(\kappa a)$ is 1.5. The measurements of Wang *et al.* were conducted using the Smoluchkowski approximation, as they sought to determine relative changes between experiments. They claimed that accurate measurements therefore are only determined when nanoparticle concentration is greater than a critical value [148].

Hotze *et al.* noted that nanoparticles conflict with fundamental assumptions of DLVO theory due to their size [145]. One of these assumptions is that interactions can be related to the forces between infinite flat surfaces. Nanoparticles have too great a surface curvature for making the assumption that $\kappa a >> 1$. Nanoparticles can also vary in their electronic structure, surface charging and reactivity owing to the high content of atoms near or on the particle-solution interface.

Progress in understanding the impact of particle size on zeta potential measurement values is growing. Abbas *et al.* used the corrected Debye-Huckel theory of surface charging for the interface, as well as Monte Carlo Simulations. Abbas *et al.* directly examined the role of particle size on surface charge density, finding that below a critical size (~ 10 nm), nanoparticles can develop greater values of surface charge [162]. This is attributed to the geometrical difference in ion distribution between a flat interface and a spherical particle. Nanoparticles with high curvature have their charge screened by a greater content of counterions and from all directions as opposed to a planar half-space, as was explained by Lyklema [163].

Abbas *et al.* showed that surface charge density increases as particle size decreases. This enhanced screening enables nanoparticles to increase the number of dissociated surface sites, raising interfacial charge. Thus, higher sur-

face charge and increased counterion screening proceed together. In addition, this theory predicts that the IEP value of nanoparticles should become higher as nanoparticle size is decreased, as the screening allows for greater dissociation of protons (i.e. enhanced surface acidity). These predictions were also observed for nanoparticles of iron oxide [138, 164] and again in TiO_2 [165, 166, 167, 168].

These expressions would suggest that nanoparticles demonstrate greater zeta potential values than bulk materials (with caveats for the shift in IEP). Prior treatment suggested that zeta potential would decrease as nanoparticle size decreased [169], and aggregation of the nanoparticles into flocs would develop greater zeta potential values. Holmberg *et al.* examined the question of how best to accurately determine the zeta potential value of nanoparticles under these models for enhanced counterion screening of the interface [165]. The Smoluchowski approximation ignores particle size and assumes a linear correlation between electrophoretic mobility and zeta potential. Holmberg found that using the accurate values for the Henry function from the Ohshima expressions and independent determination of particle size, the zeta potential value of nanoparticles was indeed greater than values determined using the Smoluchowski equation. The zeta potential results were still just a third of the expected value of the true surface charge density.

These studies have primarily been conducted with model ceramic oxide systems. Electrokinetic measurements of mixed metal oxides are often affected by the specific adsorption of divalent and trivalent cations with pH. This considers ion adsorption as either an inner sphere complex, outer sphere complex, or as a component of the diffuse double layer based on thermal motion and electrostatic attraction. In the TiO_2 system for example, studies of the adsorption of these cations found that they form inner sphere complexes generally in tetravalent coordination with four neighboring surface oxygen groups, composed of two hydroxo and two oxo species [170–172]. Surface adsorption of ionic species, especially divalent and trivalent soluble ions, can change these surface reactions by surface complexation, and thus alter charging properties at the interface [173–178]. Many divalent ions are potential-determining for TiO_2 based on this effect [179, 180, 172]. As a result, surface leaching can lead to readsorption, and drift in the zeta potential and colloidal stability with time.

The surface chemistry of multicomponent metal oxides impacts surface charge via surface acid-base properties, the adsorption behavior of surfactants, and the surface stability or leaching of cations. It is well understood that the adsorption or loss of protons from the terminating hydroxyl groups present on most oxides generates surface charge and potential. The simplest model is the 1-pKa equation based on the addition of a proton to a surface, and the partial charge of the surface hydroxyl.

$$[TiOH^{-0.5}]_s + \{H^+\}_b \rightleftharpoons [TiOH_2^{0.5}]_s \qquad (10)$$

$$K_a = \left\{ \frac{[TiOH_2^{0.5}]_s}{[TiOH^{-0.5}]_s \{H^+\}_b \exp(-z_H F \Psi_0 / RT)} \right\} \qquad (11)$$

The protonation constant of the surface group relates the concentrations of surface sites (μmoles/m^2), the bulk proton activity H^+_b, the charge of the proton z_H, Faraday's constant F, the gas constant R, absolute temperature T (K), and the surface potential Ψ_0. The multisite, ion complexation model (MUSIC) developed by Hiemstra and coworkers has shown good predictive capability for determining the surface charging of these metal oxides and their hydroxides [181–184] The evaluation of surface chemistry is modeled under the assumption that material dissolution is not active, and therefore many treatments of surface reactivity are performed on homogeneous metal oxides of low solubility, such as TiO_2, ZrO_2, Al_2O_3, SiO_2, and various iron oxides. The CD MUSIC model approach has found excellent agreement to specific adsorption of divalent and trivalent cations, with pH, ionic strength and temperatures up to and including hydrothermal reaction temperatures [171, 172, 178, 185–189]. Notable conclusions are that ion hydration energy impacts adsorption to the surface with electrostatic effects, and that raising the temperature shifts the IEP to lower values, based on the increased solvent dissociation and decreasing dielectric constant of water with temperature [187, 190–192]. The behavior of multicomponent metal oxides is complicated by the local effects of multiple cations on oxygen partial charge or polarity. Bunker predicted phase stability or surface protonation reactions using a theoretical treatment of the surface properties of mixed metal oxides based on the Pauling concept of partial charge [193]. The surface reactions of oxygen anions are affected by the local bonding of different types of cations, and charges can vary between systems.

Despite the development of the CD MUSIC treatment of oxide interfaces, there is little application of these reactions to multi-component oxide particle surfaces, such as the ABO_3 perovskites (A = Ca^{2+}, Ba^{2+}, Sr^{2+}, or Pb^{2+}; B = Ti^{4+}, Zr^{4+}). One reason for difficulty in applying these techniques is the requirement that the particles are largely insoluble during the measurement. This can prove problematic even in single-cation systems such as iron oxides. The varying oxidation states of iron can lead to thermal dissolution, as was noted by Wesolowski *et al.* for magnetite particles below the PZC, which leached Fe^{2+} from the surface [187]. In the titanate perovskites, the addition of the A site, divalent cation is expected to raise the PZC of the perovskite oxide [194]. It is likely that simulation and experimental measurement of multicomponent systems can be conducted using the CD MUSIC approach in the future. Most often in practice, the understanding of multicomponent oxide surface charging is measured and evaluated with solution conditions.

(1) Materials stability

The question remains, how can one predict the instability of cations in multication oxides? To reply, one should first consider the soluble species. Acidic conditions generally lead to fully charged ions in aqueous solution. The hydrolysis reactions of metal cations are central to understanding the point of minimum solubility. Baes and Mesmer discuss the solubility of ions over the pH range, and describe points in which hydrolysis reactions will lead to precipitates [106]. Once these conditions can be established, the phase stability of the metal oxide should be evaluated.

For instance, the hydrothermal synthesis literature can be consulted for regions of phase stability for a multicomponent oxide. If a mixed cation oxide can be directly synthesized, that indicates the potential for at least an operating region of component stability, whereas failure to identify conditions of hydrothermal synthesis suggests the lattice strain is too great to expect solution stability. Although suitable for formation by hydrothermal synthesis, $BaTiO_3$ is a well-known instance of material instability in which Ba^{2+} leaches from the surface below alkaline pH at room temperatures.

$$BaTiO_2 + 2H^+ \rightleftharpoons Ba^{2+} + TiO_2 + H_2O \quad (12)$$

The hydrothermal stability diagrams of $BaTiO_3$ and other titanate perovskites show that the thermodynamic stability of these particles is maintained only under solution conditions of high pH [195]. Electrokinetic studies on $BaTiO_3$ show that leaching is developed under acidic conditions. Much aqueous processing is preferred to be conducted under conditions closer to neutral pH values. The thermodynamic free energy for the dissolution reaction of $BaTiO_3$ is much greater than $PbTiO_3$ or $PbZrO_3$, explaining the well-known sensitivity of $BaTiO_3$ in aqueous processing [196]. Changes in surface chemistry can be attempted by compositional substitution. There are multiple substitutions possible in the (Pb, Ba, Sr, Ca)(Ti-Zr)O_3 system, for example, indicating there are reaction conditions stabilizing those materials [197]. However, studies of the instability of mixed A and B site perovskites by Lee *et al.* found that substitution of small amounts of Ca for Ba in mixed (Ba+Ca)(Zr+Ti)O_3 (BCTZ) powders would affect the degree of environmental sensitivity of the powder dissolution [40].

Another parameter for the stability of mixed cation oxides is the lattice strain in the crystal and its effect on thermodynamic properties [198]. The stability of a mixed-oxide perovskite can be evaluated with the tolerance factor, t, of the crystal structure.

$$t = (r_A + r_O)/\sqrt{2}(r_B + r_O) \quad (13)$$

These terms r_A, r_B, r_O and are the ionic radii of the A^{2+}, B^{4+} and O^{2-} ions, respectively. Tolerance factor can play a role in the success of materials synthesis that relates to oxide stability. For example, Modeshia and Walton examined the success of 50 % A site substitution in the $AMnO_3$ perovskites with tolerance factor, learning that t values of 0.9 to 1 demonstrated successful substitution of divalent cations [199]. Sahu *et al.* used the tolerance factor in understanding the surface properties of titanate perovskites [200]. They found that $BaTiO_3$ has the highest tolerance factor of 1.15 in comparison to $CaTiO_3$, $PbTiO_3$, and $SrTiO_3$. In addition, their work performed thermodynamic measurement of surface properties and found that $BaTiO_3$ has the highest surface energy of these titanate perovskites both in the nonhydrated and hydrated states (see Table 1). There is a significant energetic argument for lowering the free energy of the surface by dissolution of Ba^{2+} to develop a more TiO_2-like interface. Surface energy measurements can be a parallel indicator of the surface stability. The surface chemistry of $BaTiO_3$ must consider these factors, and in fact Blanco-Lopez stated that $BaTiO_3$ should be considered as a case of an insoluble oxide (TiO_2) containing a partially soluble inorganic salt (BaO). This system has potential-determining ions related to H^+ and Ba^{2+}, and the precipitation of the carbonate as factors to mitigate in colloidal processing.

VI. Surfactants for Complex Metal Oxides

The approach for developing a dispersion of a multicomponent metal oxide has shown that there are several factors to consider. The key properties of a dispersing moiety are the strong adsorption to the particles surface, complete coverage, a favorable wetting interaction, and an electrostatic and/or steric property suitable to developing the desired macroscopic rheological response. The dispersant is also chosen based on the needs of the manufacturing process. For example, electrophoretic deposition requires charge on the colloidal particles, and often is conducted in alcohol-based solvents to avoid the electrolysis of water into H_2 and O_2 gases. Other processes such as slip casting, gel casting or freeze casting may prefer aqueous solvents for environmental reasons, but require the formation of very high solid loading in the consolidated product. The dispersant choice is thus based on the colloidal stabilization mechanism using either electrostatic, steric, or electrosteric means. In addition, particle size matters for nanoparticle systems. Scaling the stabilization length to the particle size is an effective method to optimize colloidal properties. As the particle size *a* decreases, the effective volume of the stabilizing dispersant or range δ affects the particle packing density and rheology of the system (see Eq. 6). Studart *et al.* demonstrated the effect of interaction length with custom surfactants for alumina nanoparticles [201]. Steric dispersion with nonionic polymers allowed for a great improvement of solids loading and final properties.

Dispersant molecules are designed to include strongly adsorbing chemical moieties for adhesion to the particle surface, and either charge generating or soluble polymer structures to prevent aggregation [202]. The number of chemical moieties for adsorption to metal oxides is surprisingly limited to phosphate and phosphonate, sulfate and sulfonate, carbonyl, carboxylic acid, hydroxyls, amines and amides, although there are a number of other variations in Lewis acids or bases that could be considered. The placement and combinations of these groups on a polymer backbone or cyclohexane ring compound, however, raise the level of complexity to near infinite combinations. This makes it necessary to limit conditions for the choice of surfactants. Owing to the growth in nanoparticle processing, we shall discuss low-molecular-weight surfactants ranging from 200 to 5000 g/mol, and generally refer to aqueous systems, although mixtures with polar but non-aqueous systems are also used with some surfactants. Adam *et al.* used trioxadecanoic acid (TODA) as a suitable surface modifier for the electrosteric colloidal stabilization of zirconia nanoparticles in water, ethanol, and other dispersion media [124]. The factors controlling adsorption are similar to those properties and mechanisms for polymer adsorption, as many chemical structures incorporate multiple chemical groups as adsorbing units. For

a description of several non-aqueous systems and dispersant choice, see Raj and Cannon who review many examples of non-aqueous, electrosterically stabilized systems using common dispersants such as "fatty acids, amines, and esters" [203].

(1) Electrosteric stabilization

The use of polyelectrolytes is very common for control of particle dispersion, and due to the effects of electrical charges, there is great depth in understanding all the behavioral effects in ceramic dispersion systems [204]. Poly acrylic acid (PAA) is a commonly investigated polyelectrolyte used for many ceramic oxide systems [43, 205–218]. There are several commercial products having low molecular weight that will preferably adsorb in flat conformations, and provide electrosteric stabilization. A benefit to PAA is that the effective plane of the repulsive electrostatic charge is displaced from the surface, giving higher electrostatic stability [219]. The behavior of polyelectrolyte adsorption is related to electrostatic effects between the polyelectrolyte and the surface, and relates to the PZC of the surface. Higher adsorbed amounts are expected when the charges are opposite, and electrolyte effects can impact the adsorbed amount and polymer conformation. The use of polyelectrolytes has extensive history in colloidal processing, and many of the factors affecting behavior are intimately connected [204]. Sato *et al.* examined the application of PAA at high solids loading, in which dispersant molecular weight was decreased to 2100 g/mol to prevent high thickness steric layers on TiO_2 [220]. Minimizing viscosity showed a correlation with solids loading as expected. For TiO_2, using low molecular weight PAA that adsorbs in a flat conformation creates short-range electrosteric stabilization, and can allow for primary nanoparticle dispersions [110]. $BaTiO_3$ is well known for its solution instability and Ba^{2+} leaching, and the use of polyelectrolytes in its dispersion was recently reviewed [204, 221].

Polyelectrolytes are sensitive to the level of ionic strength in the solvent, based on electrostatic screening and counterion condensation [222, 223]. The effect of divalent and trivalent ions on anionic polyelectrolytes also has a long history of study and treatment of the interparticle forces in colloidal systems stabilized with polyelectrolyte layers [224, 225]. Counterion binding can be either purely electrostatic and allow for ion transport, or have an additional energetic interaction leading to cross-linking. In adsorbed layers, this can reduce the electrostatic component of the repulsive interaction, but also lead to thick steric layers. For example, Abraham determined that Ca^{2+} adsorption led to higher adsorption by screening of electrostatic repulsion [226]. Bell *et al.* found that Ba^{2+} cross-linked PAA surface layers, preventing collapse and maintaining a steric shell in a gelled surface layer [227].

(2) Steric stabilization

There are several cases in which the processing conditions do not provide sufficient surface potential for colloidal stability, and polymeric surfactants are sought to generate stable, high-solids-content dispersions. The function of polymer systems that provide dispersion stability is to create an osmotic barrier between particles by the adsorption of a polymer layer, such that either steric or both electrostatic and steric (electrosteric) interactions are generated. There are numerous sources for understanding the complexities of polymer layers at interfaces [228–230] Ultimately, strong stabilizing forces are expected to be generated when polymer chains are grafted at high density, such that the layers extend significantly into solution due to crowding between neighboring chains. The size of a free polymer coil is related to the average degree of polymerization n, and the segment length l. The radius of gyration R_g of the polymer can be determined with the expression:

$$R_g = \frac{l\sqrt[2]{n}}{\sqrt{6}} \tag{14}$$

When the distance between grafted chains, s, is less than the size of a free polymer coil, so-called brush layers are established. The layer thickness formed in this case can be related to degree of polymerization and grafting coverage by $L_0 = nl^{5/3}\Gamma^{1/3}$.

Polymer chains anchored to a surface, either by covalent bonding or by surface complexation mechanisms, provide a barrier to particle aggregation if a portion of the chain extends into the solvent with a range or thickness that reduces the van der Waals attraction. This occurs in the case that the solvent interaction with the polymer is favorable, and the polymer chain is well solvated. The solvent quality is often established by the χ parameter in Flory Huggins theory, which is a property of both the polymer and the solvent. The steric repulsion can be modeled for particles of radius *a*, adsorbed polymer thickness δ, and separation distance *H*, as [203]:

$$E_{Steric} = \frac{4\pi kTB\phi^2}{3}\left(\frac{1}{2}-\chi\right)\left(\delta-\frac{H}{2}\right)^2\left(3a+2\delta+\frac{H}{2}\right) \quad \text{for } H \le \delta \tag{15}$$

The development of stable suspensions of metal oxides based on steric stabilization can be conducted by growth of polymer chains from the powder surface or by grafting to reactions, but the vast majority of applications require the addition of a commercial dispersant to a separate powder. Developing strong steric stabilization is most readily done by adsorption of a strongly adherent polymer backbone such as PAA or PMAA that is functionalized with multiple chains of a second, high-solubility polymer, such as PEO in aqueous systems. These comb surfactants generate a steric repulsion that resists ionic compression. Klimkevicius *et al.* developed cationic comb polymers for TiO_2 nanoparticle dispersion at pH 10 [231], as did Rhodes *et al.* for SiO_2 surfaces [232]. There are excellent reviews of steric stabilization [230, 233, 234] and comb polymers to describe the performance of these types of surfactants in colloidal stabilization. The factors leading to comb polymer dispersants include the molecular weights of the anchor block and the polymer "teeth". Variation in these parameters have been applied by several researchers [235]. Flatt *et al.* provide a scaling expression for comb polymers that has been used for force measurements by means of colloidal probe atomic force microscopy [236]

$$\frac{F}{\kappa T} = 2\pi\left(\frac{R_1 R_2}{R_1 + R_2}\right)\frac{\rho^{-29/30} N^{-13/30}}{\alpha}$$
$$\left(\frac{5}{\sqrt[1/3]{2}} R_{AC}{}^{2/3} - \frac{1}{2} D^{-1/3}\left(3D + 4(2)^{2/3} R_{AC}\left(\frac{R_{AC}}{D}\right)^{2/3}\right)\right) \quad (16)$$

Here, R_{AC} is the radius of gyration of the core polymer (adsorbing block), P is the number of monomers in the chain, and N is the number of monomers.

These comb polymers are used in reactive systems, such as cements and concrete, which perform under highly alkaline conditions [236, 237]. Ran examined the impact of Ca^{2+} ions for cement dispersions [238, 239]. These factors translate to other reactive systems in ceramic oxides. Kirby *et al.* (2004) used PAA-PEO comb polymers for $BaTiO_3$ stabilization [240]. The primary benefit of this type of surfactant is that the steric stabilization is not ion-sensitive, unlike the PAA surfactant tested in parallel. This comb dispersant was successful over varying ionic strength and pH levels, including the addition of $BaCl_2$ as a divalent ion addition to screen electrostatic repulsion. Other comb polymers for $BaTiO_3$ have also demonstrated stabilization at pH 12, exceeding the performance of polymethylmethacrylate dispersant (Darvan C) [241].

Sakar-Deliormanli *et al.* are the only report available to our knowledge examining the impact of the dispersant upon the perovskite chemical stability (lead magnesium niobate) in dispersions [242]. They compared the effect of a PAA dispersant against a comb polymer of PAA/PEO. The carboxylate groups in the dispersants complex the Pb^{2+} and Mg^{2+} ions from the surface at pH 9, whereas the strong adsorption of the carboxylic acids in more acidic conditions led to a dense polymer layer that inhibited the divalent cation solubility. The Mg^{2+} dissolution rate is much slower than the Pb^{2+} rate.

(3) Molecular dispersants

Polymeric dispersants having molecular weight ranging from 6,000 – 15,000 serve many processing needs, yet for nanoparticle dispersion, lower molecular weight compounds can provide the short-range (electro-)steric length δ needed for aggregation control. The adsorption on surfaces as inner sphere or outer sphere complexes can be used to tether a stabilizing polymer chain and create brush layers for colloidal stability, if adhesion is strong enough. Hydroxyl- and carboxylic-acid-containing small molecules demonstrate this capability very well for several chemically inert ceramic systems. The molecular structure of the adsorbing group has significant impact in adsorption, and an extensive study on alumina surfaces was performed by Hidber *et al.* using a benzene ring as a rigid structure to control surface complexation [243]. This identified 1,2-dihydroxybenzene (catechol) and 1,2,3-trihydroxybenzene (pyrogallol) as strong adsorbing groups as pH becomes alkaline owing to the formation of a chelate surface complex. Studart further described the adsorption as a ligand exchange between surface hydroxyl groups and the -OH or $-O^-$ groups of the catechol and pyrogallol headgroups [243, 244]. There is a strong adsorption energy related to the electrostatic interactions between the surface and headgroup, and the brush density is reported to exceed the density of comb polymer surfactants. Further development of surfactants based on these headgroups demonstrated control over nanoparticle stability. Tsai *et al.* utilized pyrogallol-PEG surfactants for aqueous dispersion of Ni metal nanoparticles by electrosteric stabilization. Tsai also used these surfactants for yttria-stabilized ZrO_2 nanoparticle dispersion, leading to high packing density and > 99 % density during sintering [245].

The use of catechols as surface-adsorbing functionalities is inspired by the expression of mussel adhesive proteins, based on high content of 3,4-dihydroxy phenylalanine (DOPA), and are known to be good binding agents for inorganic surfaces [246]. The development of polyethylene glycol derivatives of various catechols has shown impressive stability for Fe_3O_4 particles [247, 248], as well as SiO_2, Nb_2O_5 and TiO_2 surfaces [249, 250]. Adsorption conditions (pH and temperature of assembly solution) strongly influenced surface coverage. For high surface coverage, a pH of the assembly solution that is close to p*K*a (near pH 6.5) of the catechol and the isoelectric point (*IEP*) of the substrate, and the temperature of the solution must be close to the cloud point for the PEG derivative. These experiments used higher molecular weight PEG, and there is the possibility that the cloud point was needed for adsorption in order to place the catechol group in proximity to the nanoparticle surface. These functionalities can be highly adhered to the surface and resist both high-temperature and salt-based exchange. It is not clear if the studied structures would provide greater chemical resistance, as studies were reported for physiological conditions or marine environments (pH 6 to 8.5), and extremes of pH were not presented. Nevertheless, functionalization of a stabilizing polymer like PEG or PVA would create high affinity surfactants for nanoparticle stabilization.

(4) Surface passivation during dispersion

Although nanoparticle dispersion has been greatly explored and related to surfactant choice, the number of studies that incorporate surface passivation is quite sparse. The primary focus of the field of dispersion chemistry has been the attainment of systems that are highly stable to aggregation, or the control over macroscopic rheological properties leading to forming techniques, including porous and 3D printed formulations. Chemical stability can be guaranteed if conditions similar to the synthesis environment are maintained, in which case the particle composition is thermodynamically stable. However, if that is not possible, the particle surface must be reacted with a passivant suitable to prevent corrosion. One approach is the formation of a sparingly soluble salt, such as sulfates or phosphates reacting with multivalent cations [251, 252]. Also, the reaction of the surface with silane coupling agents is a route to interfacial stability and dispersion [137]. This may not be an option in electronic ceramics, in which compositional purity is so important. When limiting the surface passivant to fugitive elements such as H, C, N and O, the chemistries used to synthesize precursor powders return as the potential surface reactants for interfacial passivation.

The goal of the passivation-dispersion approach is to place the proper combination of chelating and surface active groups on the surface, and thereby chemisorb with surface cations to create an insoluble surface layer. Molecules that form stable five- and six-membered rings are thought to enhance the adsorption of inhibitor agents, and inner sphere adsorption as bidentate complexes are believed to inhibit dissolution due to the difficulty of dissolving two cations together [251–253]. Based on the organic functionality, this lends to surface-active groups that include hydroxyl, amine and carboxylic acids. Clearly the combinations of organic structures is extensive, but include chelating compounds such as amino acids, polypeptides, polysaccharides, and organic di-acids and tri-acids.

Small, organic molecules with surface-active groups have been studied in many ceramic systems as dispersing agents, often based on carboxylic acids. Carboxylic acids are very common anionic systems. TiO_2 surfaces are known to react with carboxylic acid groups via dissociative reactions, resulting in a bridging-bidentate mode for formic, acetic, and propionic acids [254]. The proton from the acid reacts to form a surface -OH group, and H-bonding can play a role in adsorption strength. Citrate ion has three COOH groups, and in alumina, titania, and zirconia, it is found that two of the groups adsorb to the surface to generate a negative charge sufficient for electrostatic dispersion [243, 255, 256]. Due to its size, citric acid also has a steric component [257].

Citric acid dispersion ability is often contrasted with oxalic acid, which has been studied by several groups as an electrosteric dispersing agent and as a passivant. The group of Adair has pioneered the use of oxalic acid as the best stabilizing agent for preventing dissolution of multicomponent ceramics [258, 259]. Adair described the use of oxalic acid in processing $BaTiO_3$ [259]. The use of oxalic acid in aqueous processing allowed the $[Ba^{2+}]$ to be maintained below 10^{-4} mol L^{-1}, and prevented any surface leaching in the powder. This approach has a background in the low-solubility product of many metal oxalates, given in Table 1. Oxalic acid (HO_2CCO_2H) is a polar dianion consisting of a pair of carboxylate groups, and it is a highly adsorbing, bidentate ligand for surfaces, as well as strong former of solution complexes. The oxalate ion has two protonation constants [260].

$$C_2O_4^{2-}(aq) + H^+(aq) \rightleftharpoons HO_2CCO_2^-(aq) \qquad (17)$$
$$pK_{a1} = 1.23$$

$$HO_2CCO_2^-(aq) + H^+(aq) \rightleftharpoons HO_2CCO_2H(aq) \qquad (18)$$
$$pK_{a2} = 4.28$$

The speciation of oxalic acid relates to its acid dissociation constants, and for pH > 4, primarily the $C_2O_4^{2-}$ ion is present. Solution species are mononuclear, with oxalate coordinating as a bidentate chelate ligand and forming five-membered rings. Janos showed that the ligand complexes with divalent cation are of the order of citric acid chelate groups in solution [261].

The adsorption of oxalic acid is reported as an inner sphere complex with bidentate coordination on surfaces varying from clays [255] to Ca-Mg-containing glasses [262] to the Cr(III)-hydroxide surfaces of steel [263]. Surface hydroxyl groups are displaced by the adsorption process. The direct coordination with metal cations shows the high chemical affinity of oxalate to metal (hydr)oxide surfaces. Filius *et al.* looked at a CD-MUSIC approach to the surface adsorption of several carboxylic acid molecules on goethite [264]. It is known that the adsorbed amount will decrease as electrostatic repulsion is generated at pH > PZC, between the organic molecule and deprotonated negative surface groups. Maximum adsorption is found just below the $\log K_{a1}$ of the acid.

Oxalic acid adsorption leads to negative surface charge for a variety of ceramic systems [264–268]. Johnson *et al.* found that diacids having adsorption as inner sphere complexes developed negatively charged surfaces at pH > 3. Erdemoglu measured zeta potentials of natural magnetite with oxalate and several divalent cation species in solution. (Co, Ni, Cu, Zn, Pb, and Cd) [269] Without oxalate, these cations precipitate on the particle surface as the hydroxides above pH 6. Oxalate leads to a negative surface potential by complexation with surface iron atoms, affecting the adsorption ability of the divalent cations in solution. The zeta potential became relatively insensitive to pH above pH 5, indicating that surface reactions were effectively complete.

There are exceptions to the use of oxalic acid as a processing aid. There are elements that form soluble species with oxalic acid, including V, Fe, and Al [253, 265]. One of the main applications of oxalic acid is a rust-remover, which arises because oxalate forms water-soluble derivatives with the ferric ion. High oxalic acid concentrations can lead to excess solubility, as noted by Johnson *et al.* in the bridging between particles in dispersion of alumina [268]. Solution concentrations to cover the surface can be in the order of 10^{-4} M [263], as the surface area of the adsorbed oxalate ion is noted to be 0.7 nm^2, which is roughly half that of citric acid at 1.5 nm^2 [2, 267].

VII. Consolidation of Colloidal Ceramics

Owing to the fact that such a strong link exists between the microstructure of a material and its macroscopic properties and performance, significant effort needs to be made to control the factors and parameters that influence the microstructural characteristics. It is in the sintering stage of the overall fabrication route that the body develops the final desired microstructure. Colloidal particle systems can densify by solid-state [270–273], liquid-phase [274], and viscous [275] sintering. Overall, the reduction in surface energy as the free surfaces of initially individual and discrete particles coalesce is the major 'driving force' for densification of colloidal particles. Specifically, sintering occurs as a result of the thermodynamic driving force to minimize the Gibbs' free energy, G, of a system [276–280], including minimizing the volume, interfacial, and surface energy in the system. This reduction in energy is accomplished by atomic level diffusion processes. As sintering progresses, the surface area and free energy of the system decrease as porosity is eliminated and the overall curvature in the system decreases. These processes result in either densifi-

cation (internal grain matter is transported to the pores), coarsening of the microstructure (rearrangement of matter from various locations on pore surfaces with none to minimal decrease in pore volume), or a complex combination of multiple mechanisms. Interparticle pore shrinkage, grain boundary formation, a decrease in the total volume of the system through densification and an increase in the average size of the particles through grain growth is how, from the aspect of the microstructure, material transport manifests itself during sintering.

Owing to the fact that such a strong link exists between the microstructure of a ceramic and its macroscopic electrical properties, significant efforts need to be made to control the factors that influence the characteristics of the microstructure, including the grain size distribution, grain boundary characteristics, porosity, etc. Optimized conditions, initial particle sizes, tailored sintering schedules, and specific chemical compositions need to be determined based on the macroscopic property needs for a particular application or use. In some cases the differences in grain growth and densification kinetics can be exploited to produce a desired and optimized macroscopic property.

In some situations, an optimized microstructure may require the complete elimination of porosity and the maintenance of a discrete grain size or grain size distribution. Hot pressing, hot forging, spark plasma (field-assisted) sintering and/or isostatic hot pressing are typically employed as a sintering technique to achieve these results. These techniques can provide more control over densification relative to coarsening during sintering. This is because the pressure and/or applied electric field now provides a major part of the driving force to eliminate porosity and densify the microstructure as desired. Spark plasma sintering or field-assisted sintering is a novel technique for achieving specific engineered and tailored microstructures that may or may not be achievable with conventional sintering techniques.

It should also be mentioned that it is not always possible to obtain a minimal porosity body by means of 'pressureless sintering', or sintering at atmospheric pressure. Using the example of the oxalate chemically prepared doped ZnO from earlier in this review, the electrical characteristics of ZnO varistor materials are related to their detailed microstructure. Three main microstructural features are especially important for determining their performance:

1. Doped ZnO grain size, grain size distribution, and morphology: responsible for the conductivity in the material, especially in the 'up-turn' region of the current-voltage behavior.
2. Grain boundary character: provide barriers to electrical conduction and produce the nonlinear properties.
   a. The breakdown voltage of each individual interface depends on the microstructure of that interface.
   b. The electrical characteristics are based on the type of interfaces and the grain size distribution as this determines the number of barriers to conduction.
3. Intergranular network of bismuth-rich phases
   a. The bismuth-rich phases form a network that contributes an additional current path.
   b. This path circumvents the barriers at the ZnO grain interfaces and can contribute significantly to the conductivity in the pre-breakdown region.

These features constitute the *functional microstructure* that is a result of the synthesis and forming techniques used for component fabrication and develops into maturity during sintering and densification. As for most ZnO varistor compositions, the composition used in this study developed a microstructure containing ZnO grains and various bismuth-rich phases (see Table 3). The samples prepared for this case study were dry-pressed discs that all had a similar initial microstructure and an 'as-pressed' density of 2.85 ± 0.02 g/cm^3. The samples were sintered following either thermal profile "A" or thermal profile "B" as listed in Table 4. These schedules generated sintered samples that were almost fully dense yet possessed a unique microstructure in comparison.

Table 3: Additives and dopants used in this ZnO-based varistor composition for tailoring the microstructure and the electrical behavior.

Additive/Dopant	Role	Mol%
ZnO	Conductive grains	98.94
Bi_2O_3	Non-linearity (α) inducer	0.56
CoO	Non-linearity (α) enhancer	0.25
MnO_2	Non-linearity (α) enhancer	0.25
Al	Non-linearity (α) enhancer	~300 ppm
Na	Reliability enhancer	~300 ppm

The two distinct thermal profiles were chosen to verify and establish the link between the matured functional microstructure and the electrical behavior of the material. The goal here was to prove the hypothesis that the electrical behavior of the material, voltage-current relationship in the 'switch' region, is a direct function of the final functional microstructure. Electrical measurements were performed on samples prepared from the same powder and then sintered to either the schedule "A" or schedule "B". The results from the electrical characterization are shown in Fig. 5. The figure shows that for both schedules the switch field decreased as the maximum sintering temperature increased. It also indicates the nature of that relationship is unique based on the schedule and independent of the maximum sintering temperature. These results establish and verify the link between the functional microstructure and electrical properties.

It has been shown, through this case study, that the detailed microstructure of the ZnO varistor material is strongly dependent upon the fabrication variables, from colloidal synthesis through densification by sintering. The electrical properties of these materials are directly influenced by the development of the functional microstruc-

ture. This shows that material stability in multication colloidal processing is even more critical, in which microstructural development is directly impacted by atomic scale control throughout the colloidal processing process.

(1) Nonconventional materials systems – spark plasma sintering

Spark plasma sintering (SPS), as the name suggests, utilizes a spark plasma or plasma discharge to provide thermal energy for solid-state sintering. It also involves high electrical current to provide field-assisted sintering, depending on different stages during an SPS process. The major merits for SPS include rapid heating and cooling, higher densification rate and shorter sintering time, all of which are superior to conventional solid-state sintering methods. Many materials prepared with SPS have shown exceptional properties compared to other sintering techniques and some novel materials have been obtained.

Fig. 6 shows a typical schematic of the SPS setup. It has a uniaxial press structure with pulsed DC current applied through the upper and lower punches. A conductive cylindrical graphite die is generally used for powder loading. The inside of the graphite wall is lined with graphite foil or boron nitride (BN) spray for easier demolding. The sintering temperature is controlled by voltage-current (V-I) output power and monitored by a thermocouple or pyrometer. The field-assisted sintering process consists of several phases. During the initial phase, a plasma charge is pervasive in a gap between dry compressed particles. As a result, a large amount of heat is generated momentarily, leading to the softening or melting at the particle surface, which further bridges the gap and forms the necks in contact areas. Then, the effect of resistance heating ceases when the second phase is initiated, the Joule heating. Current through the particles, and together with the thermal energy generated at the first stage, contributes to a rapid ramping to the sintering plateau within a relative short time period (usually within minutes). The applied pressure further facilitates the plastic flow and densification. The different phases of SPS are illustrated in Fig. 7.

Table 4: Sintering profiles "A" and "B" to a maximum sintering temperature of XXX °C.

Thermal Profile "A"	Thermal Profile "B"
RT to XXX °C at 3 °C/min and hold for 16 h	RT to 500 °C at 3 °C/min and hold for 2 h
XXX °C to 400 °C at 1.5 °C/min	500 °C to 675 °C at 1 °C/min and hold for 2 h
400 °C to 100 °C at 3 °C/min	675 °C to 700 °C at 0.5 °C/min and hold for 2 h
	700 °C to XXX °C at 0.5 °C/min and hold for 16 h
	400 °C to 100 °C at 3 °C/min

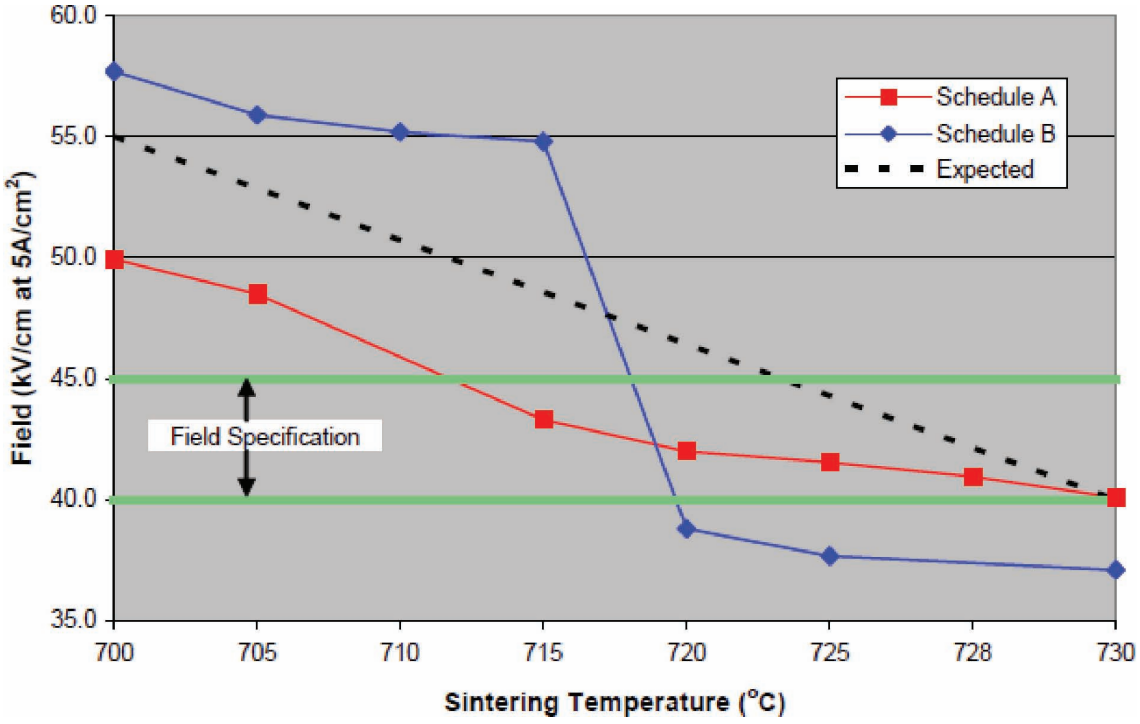

Fig. 5: Effects of maximum sintering temperature on electric field.

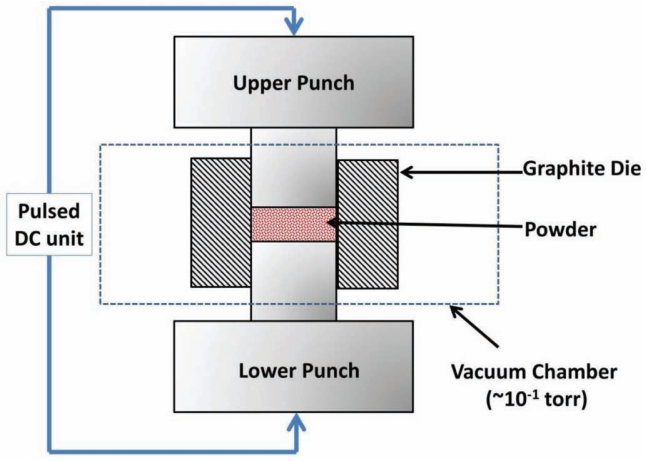

Fig. 6 : The sketch diagram of the spark plasma sintering (SPS) setup.

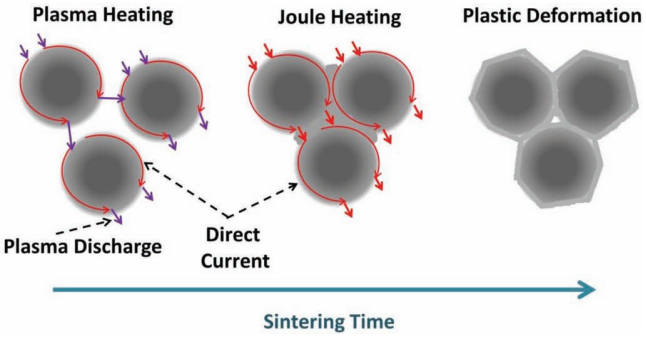

Fig. 7 : The general sintering mechanisms of SPS in respect of sintering time.

In addition to the characteristic fast sintering and high densification of SPS, the field effects on grain growth, grain orientation and grain boundary migration are very intriguing. It would be generally considered that a higher heating rate or shorter sintering time would constrain excessive grain growth, yielding smaller fine grains. However, this is not always the case. Research on transparent alumina has shown that higher heating rate would yield larger grain size, when overheating is not taken into account [281]. This anomaly might result from the inherent complexity of SPS processing, such as field-assisted mass transport, plastic deformation coupled with plasma charge, thermal gradient, etc. Preferred orientation is also observed in some materials prepared by means of SPS [282–284]. On one hand, the liquid phase and the shear stress under uniaxial pressure is helpful in oriented grain growth or crystallite alignment. On the other hand, the momentary high temperature generated by plasma charge would create a lowered plastic yielding and facilitate plastic deformation under uniaxial pressure. Also superplasticity behavior in some ceramics is more likely to be observed from SPS owing to its high temperature capability. With regard to grain boundary and migration, field-assisted sintering has been widely studied with well-established kinetic models to describe the electrical field on driving force and growth rate [285, 286]. Generally speaking, the applied field would interact with the space charge adjacent to the grain boundary, thus modifying the grain boundary energy and ion diffusion near or at the grain boundary.

SPS has been utilized to fabricate various kinds of ceramics, including transparent ceramics, ceramic composites and other oxides that require high sintering temperature and high densification. The following are a few examples that illustrate that:

Example #1: SPS is a suitable for the densification of composite materials as shown in the case of sintering oxides and carbide dispersed zirconia inert matrix fuels (ZrO_2 77 wt % – ZrC 15 wt% – CeO_2 5 wt% – Er_2O_3 3 wt%) [27]. Oxide and carbide materials are generally difficult to sinter via conventional sintering, which involves large energy consumption and time effort. SPS is an effective tool to consolidate ceramic composites to nearly fully densified samples. Fig. 8 shows the actual piston/punch speed as a function of sintering time, from which the stage of sample shrinkage can be revealed. This behavior is a combinational effect from plasma discharge, degree of plastic deformation, and thermal activation energy. SPS was able to densify this composite in only 10 min dwelling at 1300 °C.

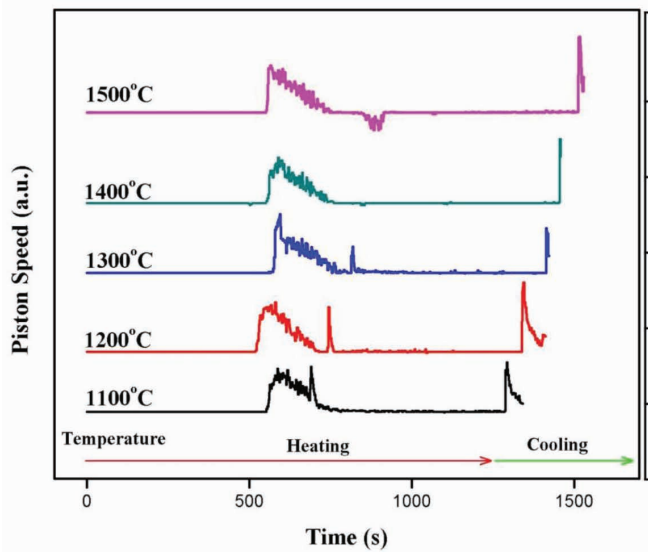

Sintering Temperature (° C)	Relative Density (%)
1100° C	87.6057
1200° C	98.8557
1300° C	99.47211
1400° C	99.9340
1500° C	99.4323

Fig. 8 : Piston speed recorded during SPS sintering, indicating the desynchronized densification at different sintering temperatures.

Example #2: For some classic electronic ceramics such as barium titanate, SPS has also exhibited great potential in obtaining samples with small grain size yet high density. Fig. 9 is an example of SPS barium titanate. The submicron grain size and ~ 96 % relative density was obtained in only 5 minutes at 850 °C.

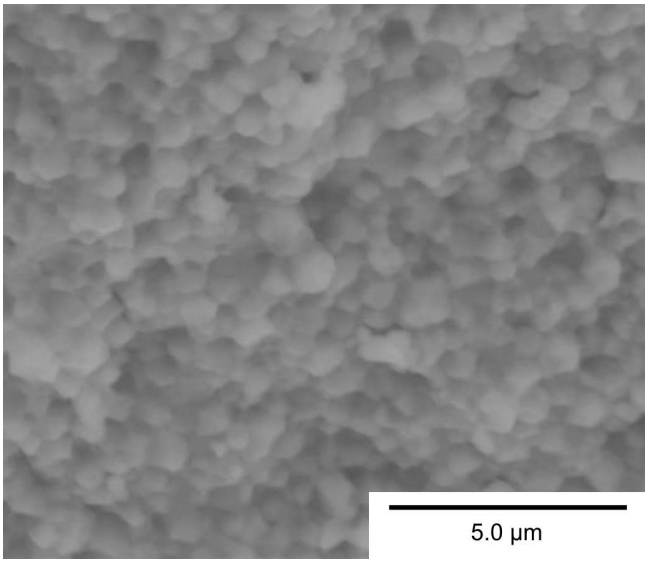

Fig. 9 : SEM micrographs of barium titanate ceramic.

Example #3: In most cases SPS is used for sintering or consolidation purposes, however, it is also capable of *in-situ* sintering, namely, reactive sintering. Our recent study examined the capability of SPS reactive sintering of $CuAlO_2$. $CuAlO_2$ is a very attractive p-type transparent conducting oxide in many emerging applications. However, the performance and phase purity are highly dependent on processing techniques. Conventional synthesis from chemical solution and solid-state reaction might involve high temperature, repeated heat treatment, and sophisticated experiment control. Spark plasma sintering, on the other hand, can synthesize and densify pure $CuAlO_2$ via a single step within relatively short time period. The inherent low vacuum enabled by the SPS is thermodynamically favorable for the solid-state reaction of $CuAlO_2$ from CuO and Al_2O_3. Nevertheless, the direct sintering of $CuAlO_2$ powders through SPS can be challenging since the redox reaction of Cu is severe. The CuO and Al_2O_3 were well mixed and loaded into the graphite die. The as-sintered disc exhibited pure delafossite $CuAlO_2$ phase (Fig. 10(a)) and nanoscale microstructures (Fig. 10(b)).

Spark plasma sintering (SPS) has been widely acknowledged as an effective method to sinter ceramics. The discharge plasma and successive Joule heating could significantly facilitate plastic deformation under pressure, resulting in dense ceramic bodies within a short time. The samples as-sintered by means of this activated sintering usually exhibit smaller grain size, higher density, good mechanical properties and sometimes preferred orientations compared to conventional solid-state sintering. In addition, the utilizations of electrical discharge and electrical field give rise to new studies on corresponding sintering rate and mass transport. Here, we have shown several examples of sintering via SPS and demonstrated the great potential of using this technique in the area of optical ceramics, composites, electronic ceramics and *in situ* sintering.

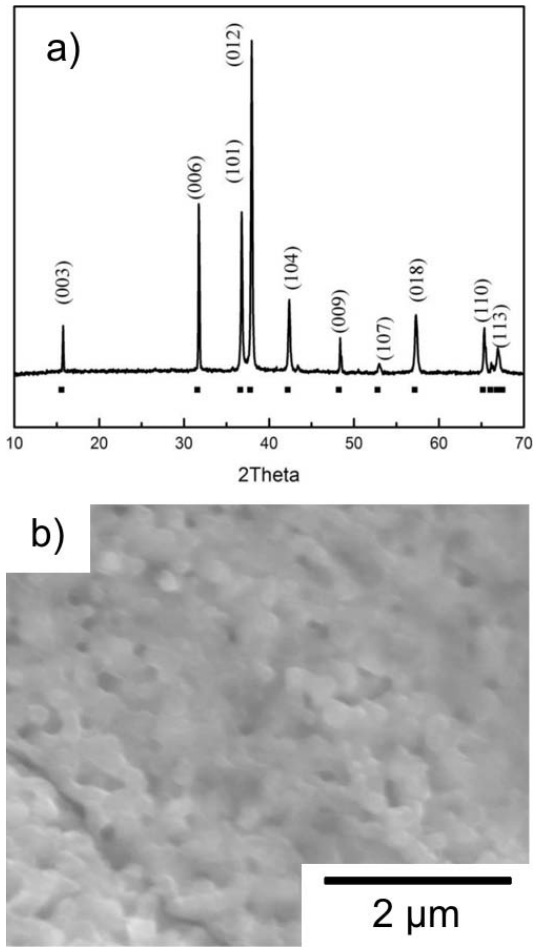

Fig. 10 : (a) XRD pattern of $CuAlO_2$ synthesized via reactive SPS sintering; (b) SEM micrograph of as-sintered $CuAlO_2$ bulk sample..

VIII. Summary and Conclusions

Advanced ceramic oxide electronic devices require the ability to optimize and tailor the properties of a colloidal particle system into the final component with the desired and optimized microstructure that links properties with performance. All aspects of ceramic preparation and processing are important to the final properties of the ceramic component. The strategy to achieve optimal material performance in colloidal multicomponent electronics is based on a scientific understanding of the material synthesis process, interfacial stability in colloidal processing, and control over final microstructure by advanced sintering processing. The need to understand the interface of colloidal materials and control surface reactions is paramount to maintaining the chemical homogeneity that impacts the development of sintered microstructure. The thermodynamic conditions to chemically prepare a desired ceramic oxide lead directly to methods suitable to control and passivate that material interface. In the event that these conditions cannot be maintained, concepts to passivate the interface with fugitive organic additives are reviewed, so that sintered microstructures can be best controlled.

Acknowledgements

The authors sincerely thank Mike Winter, Pin Yang, Tom Chavez, Lonnie Haden, Julie Gibson, Lindsey Evans, Steve Lockwood, and Kevin Ewsuk. T.C.M. would like to acknowledge Jean L. Leger, Tyler E. Stevens, and David A. Vargas for assistance with nanoparticle synthesis and electron microscopy. T.C.M. acknowledges partial support from the Air Force Research Laboratory, Directed Energy Directorate, High Power Microwave Division (AFRL/RDH).

Sandia National Laboratories is a multi-program laboratory operated by Sandia Corporation, a wholly owned subsidiary of Lockheed Martin Corporation, for the U.S. Department of Energy's National Nuclear Security Administration under contract DE-AC04 – 94AL85000.

References

1 Bergstrom, L.: Colloidal processing of ceramics. In: Handbook of applied science and colloid chemistry, Holmberg, K., Ed. John Wiley & Sons, Ltd., 2001.

2 Bergstrom, L., Schilling, C.H., Aksay, I.A.: Consolidation behavior of flocculated alumina suspensions, *J. Am. Ceram. Soc.,* **75**, [12], 3305 – 3314, (1992).

3 Aksay, I.A.: Microstructure control through colloidal consolidation. In: Advances in ceramics, forming of ceramics, Mangels, J.A., Messing, G.L., Eds. American Ceramic Society: Columbus, OH, 1984; Vol. 9, 94 – 104.

4 Lange, F.F.: Powder processing science and technology for increased reliability, *J. Am. Ceram. Soc.,* **72**, [1], 3 – 15, (1989).

5 Ferrari, B., Moreno, R.: EPD kinetics: A review, *J. Eur. Ceram. Soc.*, **30**, [5], 1069 – 1078, (2010).

6 Besra, L., Liu, M.: A review on fundamentals and applications of electrophoretic deposition (EPD), *Prog. Mater. Sci.,* **52**, [1], 1 – 61, (2007).

7 Yang, J., Yu, J., Huang, Y.: Recent developments in gelcasting of ceramics, *J. Eur. Ceram. Soc.*, **31**, [14], 2569 – 2591, (2011).

8 Cesarano, J.: A review of robocasting technology. In: Solid freeform and additive fabrication, Dimos, D., Danforth, S.C., Cima, M.J., Eds. 1999; Vol. 542, 133 – 139.

9 Tallon, C., Franks, G.V.: Recent trends in shape forming from colloidal processing: A review, *J. Ceram. Soc. Jpn.,* **119**, [1387], 147 – 160, (2011).

10 Li, W.L., Lu, K., Walz, J.Y.: Freeze casting of porous materials: review of critical factors in microstructure evolution, *Int. Mater. Rev.,* **57**, [1], 37 – 60, (2012).

11 Yu, J., Yang, J., Huang, Y.: The transformation mechanism from suspension to green body and the development of colloidal forming, *Ceram. Int.*, **37**, [5], 1435 – 1451, (2011).

12 Deckers, J., Vleugels, J., Kruthl, J.P.: Additive manufacturing of ceramics: A review, *J. Ceram. Sci. Tech.,* **5**, [4], 245 – 260, (2014).

13 Conrad, J.C., Ferreira, S.R., Yoshikawa, J., Shepherd, R.F., Ahn, B.Y., Lewis, J.A.: Designing colloidal suspensions for directed materials assembly, *Curr. Opin. Colloid. In.,* **16**, [1], 71 – 79, (2011).

14 Lewis, J.A.: Colloidal processing of ceramics, *J. Am. Ceram. Soc.*, **83**, [10], 2341 – 2359, (2000).

15 Sigmund, W.M., Bell, N.S., Bergstrom, L.: Novel powder – processing methods for advanced ceramics, *J. Am. Ceram. Soc.*, **83**, [7), 1557 – 1574, (2000).

16 Snyder, G.J., Haile, S.M.: Fuel cell materials and components, *Advanced Materials for Energy Conversion II*, 33 – 41, (2004).

17 Jung, W., Gu, K.L., Choi, Y., Haile, S.M.: Robust nanostructures with exceptionally high electrochemical reaction activity for high temperature fuel cell electrodes, *Energ. Environ. Sci.,* **7**, [5], 1685 – 1692, (2014).

18 Keane, M.A.: Ceramics for catalysis, *J. Mater. Sci.,* **38**, [23], 4661 – 4675, (2003).

19 Yang, C.K., Yamazaki, Y., Aydin, A., Haile, S.M.: Thermodynamic and kinetic assessments of strontium-doped lanthanum manganite perovskites for two-step thermochemical water splitting, *J. Mater. Chem. A,* **2**, [33], 13612 – 13623, (2014).

20 Yanying, W., Weishen, Y., Caro, J., Haihui, W.: Dense ceramic oxygen permeable membranes and catalytic membrane reactors, *Chem. Eng. J.,* **220**, 185 – 203, (2013).

21 Pena, M.A., Fierro, J.L.G.: Chemical structures and performance of perovskite oxides, *Chem. Rev.,* **101**, [7], 1981 – 2017, (2001).

22 Ceramic powder science, advances in ceramics. The American Ceramic Society: Columbus, OH, 1987, Vol. 21.

23 Ceramic powder science II, The American Ceramic Society: Columbus, OH, 1988.

24 Ceramic powder processing science. Deutsche Keramische Gesellschaft: Cologne, Germany, 1989.

25 Ceramic powder science IV, The American Ceramic Society: Columbus, OH, 1992.

26 Sugita, K.: The colloidal process – a new approach to advanced ceramics, *Adv. Mater.,* **4**, [9], 582 – 586, (1992).

27 Rohrer, G.S., Affatigato, M., Backhaus, M., Bordia, R.K., Chan, H.M., Curtarolo, S., Demkov, A., Eckstein, J.N., Faber, K.T., Garay, J.E., Gogotsi, Y., Huang, L., Jones, L.E., Kalinin, S.V., Lad, R.J., Levi, C.G., Levy, J., Maria, J.-P., Mattos, L., Jr., Navrotsky, A., Orlovskaya, N., Pantano, C., Stebbins, J.F., Sudarshan, T.S., Tani, T., Weil, K.S.: Challenges in ceramic science: A report from the workshop on emerging research areas in ceramic science, *J. Am. Ceram. Soc.*, **95**, [12], 3699 – 3712, (2012).

28 Stenger, F., Mende, S., Schwedes, J., Peukert, W.: The influence of suspension properties on the grinding behavior of alumina particles in the submicron size range in stirred media mills, *Powder Technol.,* **156**, [2 – 3], 103 – 110, (2005).

29 Andersson, K.M., Bergstrom, L.: Oxidation and dissolution of tungsten carbide powder in water, *Int. J. Refract. Met. H.,* **18**, [2 – 3], 121 – 129, (2000).

30 Zhang, P., Navrotsky, A., Guo, B., Kennedy, I., Clark, A.N., Lesher, C., Liu, Q.: Energetics of cubic and monoclinic yttrium oxide polymorphs: phase transitions, surface enthalpies, and stability at the nanoscale, *J. Phys. Chem. C,* **112**, [4], 932 – 938, (2008).

31 Navrotsky, A.: Nanoscale effects on thermodynamics and phase equilibria in oxide systems, *Chemphyschem,* **12**, [12], 2207 – 2215, (2011).

32 Lilova, K., Pearce, C., Rosso, K., Navrotsky, A.: Energetics of iron spinels at bulk and nanoscale, *Abstr. Pap. Am. Chem. S.,* **244**, (2012).

33 Leitner, J., Vonka, P., Sedmidubsky, D., Kamradek, M.: Nanosizing as a way to enhanced solubility of transition metals in ZnO, *J. Nanopart. Res.,* **15**, [3], (2013).

34 Esch, T.R., Gadaczek, I., Bredow, T.: Surface structures and thermodynamics of low-index of rutile, brookite and anatase – a comparative DFT study, *Appl. Surf. Sci.*, **288**, 275 – 287, (2014).

35 Bloch, L., Kauffmann, Y., Pokroy, B.: Size effect on the short range order and the crystallization of nanosized amorphous alumina, *Cryst. Growth Des.,* **14**, [8], 3983 – 3989, (2014).

36 Greenwood, R., Bergstrom, L.: Electroacoustic and rheological properties of aqueous Ce.ZrO_2 (Ce-TZP) suspensions, *J. Eur. Ceram. Soc.*, **17**, 537 – 548, (1997).

37 Greenwood, R. Kendall, K.: Acoustophoretic studies of aqueous suspensions of alumina and 8 mol% yttria-stabilised zirconia powders, *J. Eur. Ceram. Soc.*, **20**, [1], 77 – 84, (2000).

[38] Coreno, J., Coreno, O.: Evaluation of calcium titanate as apatite growth promoter, *J. Biomed. Mater. Res. A*, **75**, [2], 478 – 484, (2005).

[39] Paik, U., Lee, S., Hackley, V.A.: Influence of barium dissolution on the electrokinetic properties of colloidal $BaTiO_3$ in an aqueous medium, *J. Am. Ceram. Soc.*, **86**, [10], 1662 – 1668, (2003).

[40] Lee, J., Lee, S., Hackley, V.A., Paik, U.: Influence of [Ba +Ca]/[Ti +Zr] ratio on the interfacial property of $(Ba,Ca)(Ti,Zr)O_3$ (BCTZ) powders in an aqueous medium, *J. Am. Ceram. Soc.*, **86**, [6], 1034 – 1036, (2003).

[41] Deliormanli, A.M., Celik, E., Polat, M.: The isoelectric point of lead magnesium niobate, *J. Am. Ceram. Soc.*, **90**, [10], 3314 – 3317, (2007).

[42] Luo, L., Rossell, M.D., Xie, D., Erni, R., Niederberger, M.: Microwave-assisted nonaqueous sol-gel synthesis: from Al:ZnO nanoparticles to transparent conducting films, *ACS Sustain. Chem, Eng.*, **1**, [1], 152 – 160, (2013).

[43] Bell, N.S., Cesarano, J., Voigt, J.A., Lockwood, S.J., Dimos, D.B.: Colloidal processing of chemically prepared zinc oxide varistors. part I: milling and dispersion of powder, *J. Mater. Res.*, **19**, [05], 1333 – 1340, (2004).

[44] Carter, C.B., Norton, M.G.: Ceramic materials science and engineering. Springer, New York, 2007.

[45] Loehman, R.: Characterization of ceramics. Momentum Press, New York, 2010.

[46] Rao, C.N.R., Gopalakrishnan, J.: Synthesis of complex metal oxides by novel routes, *Acc. Chem. Res.*, **20**, [6), 228 – 235, (1987).

[47] Pithan, C., Hennings, D., Waser, R.: Progress in the synthesis of nanocrystalline $BaTiO_3$ powders for MLCC, *Int. J. Appl. Ceram.Tec.*, **2**, [1], 1 – 14, (2005).

[48] Templeton, L.K., Pask, J.A.: Formation of $BaTiO_3$ from $BaCO_3$ and TiO_2 in air and in CO_2, *J. Am. Ceram. Soc.*, **42**, [5], 212 – 216, (1959).

[49] Gateshki, M., Petkov, V., Williams, G., Pradhan, S.K., Ren, Y.: Atomic-scale structure of nanocrystalline ZrO_2 prepared by high-energy ball milling, *Phys. Rev. B*, **71**, [22], 224107, (2005).

[50] Koch, C.C.: The synthesis and structure of nanocrystalline materials produced by mechanical attrition: A review, *Nanostruct. Mater.,* **2**, [2], 109 – 129, (1993).

[51] Strobel, R., Pratsinis, S.E.: Flame aerosol synthesis of smart nanostructured materials, *J. Mater. Chem.*, **17**, [45], 4743 – 4756, (2007).

[52] Patil, K.C., Aruna, S.T., Mimani, T.: Combustion synthesis: an update, *Curr. Opin. Solid St. M.*, **6**, [6], 507 – 512, (2002).

[53] Qian, L., Zhang, H.: Controlled freezing and freeze drying: A versatile route for porous and micro-/nano-structured materials, *J. Chem. Technol. Biot.*, **86**, [2], 172 – 184, (2011).

[54] Somiya, S., Roy, R.: Hydrothermal synthesis of fine oxide powders, *B. Mater. Sci.*, **23**, [6], 453 – 460, (2000).

[55] Peterson, J.H.: Process for producing insoluble titanates, (1940).

[56] Bao, N., Shen, L., Srinivasan, G., Yanagisawa, K., Gupta, A.: Shape – controlled monocrystalline ferroelectric barium titanate nanostructures: From nanotubes and nanowires to ordered nanostructures, *J. Phys. Chem.C*, **112**, [23], 8634 – 8642, (2008).

[57] Joshi, U.A., Lee, J.S.: Template-free hydrothermal synthesis of single-crystalline barium titanate and strontium titanate nanowires, *Small*, **1** (12], 1172 – 1176, (2005).

[58] Xu, H., Gao, L.: Tetragonal nanocrystalline barium titanate powder: preparation, characterization, and dielectric properties, *J. Am. Ceram. Soc.*, **86**, [1], 203 – 205, (2003).

[59] Kolen'ko, Y.V., Kovnir, K.A., Neira, I.S., Taniguchi, T., Ishigaki, T., Watanabe, T., Sakamoto, N., Yoshimura, M.: A novel, controlled, and high-yield solvothermal drying route to nanosized barium titanate powders, *J. Phys. Chem. C*, **111**, [20], 7306 – 7318, (2007).

[60] Kwon, S.-G., Park, B.-H., Choi, K., Choi, E.-S., Nam, S., Kim, J.-W., Kim, J.-H.: Solvothermally synthesized tetragonal barium titanate powders using H_2O/EtOH solvent, *J. Eur. Ceram. Soc.*, **26**, [8], 1401 – 1404, (2006).

[61] Wei, X., Xu, G., Ren, Z., Wang, Y., Shen, G., Han, G.: Synthesis of highly dispersed barium titanate nanoparticles by a novel solvothermal method, *J. Am. Ceram. Soc.,* **91**, [1], 315 – 318, (2008).

[62] Modeshia, D.R., Walton, R.I.: Solvothermal synthesis of perovskites and pyrochlores: crystallisation of functional oxides under mild conditions, *Chem. Soc. Rev.*, **39**, [11], 4303 – 4325, (2010).

[63] Lencka, M.M., Riman, R.E.: Thermodynamic modeling of hydrothermal synthesis of ceramic powders, *Chem. Mater.,* **5**, [1], 61 – 70, (1993).

[64] Łencka, M.M., Riman, R.E.: Synthesis of lead titanate: Thermodynamic modeling and experimental verification, *J. Am. Ceram. Soc.*, **76**, [10], 2649 – 2659, (1993).

[65] Lencka, M.M., Anderko, A., Riman, R.E.: Hydrothermal precipitation of lead zirconate titanate solid solutions: thermodynamic modeling and experimental synthesis, *J. Am. Ceram. Soc.*, **78**, [10], 2609 – 2618, (1995).

[66] Lencka, M.M., Nielsen, E., Anderko, A., Riman, R.E.: Hydrothermal synthesis of carbonate-free strontium zirconate: thermodynamic modeling and experimental verification, *Chem. Mater.*, **9**, [5], 1116 – 1125, (1997).

[67] Lencka, M.M., Oledzka, M., Riman, R.E.: Hydrothermal synthesis of sodium and potassium bismuth titanates, *Chem. Mater.*, **12**, [5], 1323 – 1330, (2000).

[68] Lencka, M.M., Riman, R.E.: Thermodynamics of the hydrothermal synthesis of calcium titanate with reference to other alkaline-earth titanates, *Chem. Mater.*, **7**, [1], 18 – 25, (1995).

[69] Han, X., Zhang, D., Zhong, Z., Yang, F., Wei, N., Zheng, K., Li, Z., Gao, Y.: Theoretical design and experimental study of hydrothermal synthesis of $KNbO_3$, *J. Phys. Chem. Solids,* **69**, [1], 193 – 198, (2008).

[70] Roy, R.: Ceramics by the solution-sol-gel route, *Science*, **238**, [4834], 1664 – 1669, (1987).

[71] Messing, G.L., Minehan, W.T.: Synthesis of ceramic powders from metal alkoxides, *Nippon Seram. Kyo. Gak.*, **99**, [10], 1036 – 1046, (1991).

[72] Mazdiyasni, K.S.: Powder synthesis from metal-organic precursors, *Ceram. Int.*, **8**, [2], 42 – 56, (1982).

[73] Lal, B., Raghunandan, M.K., Gupta, M., Singh, R.N.: Electrocatalytic properties of perovskite-type obtained by a novel stearic acid sol-gel method for electrocatalysis of evolution in KOH solutions, *Int. J. Hydrogen Energ.*, **30**, [7], 723 – 729, (2005).

[74] Wang, X., Li, D., Lu, L., Wang, X.: Synthesis of substituted M- and W-type barium ferrite nanostructured powders by stearic acid gel method, *J. Alloy. Compd.*, **237**, [1 – 2], 45 – 48, (1996).

[75] Xiong, G., Zhi, Z., Yang, X., Lu, L., Wang, X.: Characterization of perovskite-type $LaCoO_3$ nanocrystals prepared by a stearic acid sol-gel process, *J. Mater. Sci. Lett.*, **16**, [13], 1064 – 1068, (1997).

[76] Shimizu, Y., Murata, T.: Sol-gel synthesis of perovskite-type lanthanum manganite thin films and fine powders using metal acetylacetonate and poly(vinyl alcohol), *J. Am. Ceram. Soc.,* **80**, [10], 2702 – 2704, (1997).

[77] Salomonsson, P., Griffin, T., Kasemo, B.: Oxygen desorption and oxidation – reduction kinetics with methane and carbon monoxide over perovskite type metal oxide catalysts, *Appl. Catal. A*, **104**, [2], 175 – 197, (1993).

[78] Morgan, D., Maric, M., Luss, D., Richardson, J.T.: Preparation of 1-2-3 superconductors from hydroxide-carbonate coprecipitation, *J. Am. Ceram. Soc.*, **73** [12], 3557 – 3561, (1990).

[79] Keshavaraja, A., Ramaswamy, A.: A comparative study of $LaCoO_3$ prepared by various wet chemical methods, *Indian J. Eng. Mater. S.,* **1**, 229 – 229, (1994).

[80] Vidyasagar, K., Gopalakrishnan, J., Rao, C.N.R.: A convenient route for the synthesis of complex metal oxides employing solid-solution precursors, *Inorg. Chem.*, **23**, [9], 1206 – 1210, (1984).

[81] Teraoka, Y., Nanri, S., Moriguchi, I., Kagawa, S., Shimanoe, K., Yamazoe, N.: Synthesis of manganite perovskites by reverse homogeneous precipitation method in the presence of alkylammonium cations, *Chem. Lett.*, **29**, [10], 1202 – 1203, (2000).

[82] Niederberger, M.: Nonaqueous sol-gel routes to metal oxide nanoparticles, *Acc. Chem. Res.*, **40** [9], 793 – 800, (2007).

[83] Niederberger, M., Garnweitner, G., Buha, J., Polleux, J., Ba, J., Pinna, N.: Nonaqueous synthesis of metal oxide nanoparticles: review and indium oxide as case study for the dependence of particle morphology on precursors and solvents, *J. Sol-Gel Sci. Technol.*, **40**, [2 – 3], 259 – 266, (2006).

[84] Monson, T.C., Rodriguez, M.A., Leger, J.L., Stevens, T.E., Huber, D.L.: A simple low-cost synthesis of brookite TiO_2 nanoparticles, *J. Mater. Res.*, **28**, [03], 348 – 353, (2013).

[85] Wei, X., Xu, G., Ren, Z., Shen, G., Han, G.: Room-temperature synthesis of $BaTiO_3$ nanoparticles in large batches, *J. Am. Ceram. Soc.,*. **91**, [11], 3774 – 3780, (2008).

[86] Yoon, S., Baik, S., Kim, M.G., Shin, N., Kim, I.: Synthesis of tetragonal barium titanate nanoparticles via alkoxide-hydroxide sol-precipitation: effect of water addition, *J. Am. Ceram. Soc.*, **90**, [1], 311 – 314, (2007).

[87] Tao, A.R., Niesz, K., Morse, D.E.: Bio-inspired nanofabrication of barium titanate, *J. Mater. Chem.*, **20**, [37], 7916 – 7923, (2010).

[88] Oskam, G., Nellore, A., Penn, R.L., Searson, P.C.: The growth kinetics of TiO_2 nanoparticles from titanium(IV) alkoxide at high water/titanium ratio, *J. Phys. Chem. B*, **107**, [8], 1734 – 1738, (2003).

[89] Turova, N.Y., Turevskaya, E.P., Kessler, V.G., Yanovskaya, M.I.: The chemistry of metal alkoxides. Kluwer Academic Publishers: New York, New York, 2002.

[90] Bradley, D.C.: Metal alkoxides as precursors for electronic and ceramic materials, *Chem. Rev.*, **89**, [6], 1317 – 1322, (1989).

[91] Yoon, S., Baik, S., Kim, M.G., Shin, N.: Formation mechanisms of tetragonal barium titanate nanoparticles in alkoxide-hydroxide sol-precipitation synthesis, *J. Am. Ceram. Soc.*, **89**, 1816 – 1821, (2006).

[92] Moure, A., Tartaj, J., Moure, C.: Synthesis and low-temperature sintering of Gd-doped CeO_2 ceramic materials obtained by a coprecipitation process, *J. Am. Ceram. Soc.*, **92**, [10], 2197 – 2203, (2009).

[93] Overs, A., Riess, I.: Properties of the solid electrolyte gadolinia-doped ceria prepared by thermal decomposition of mixed cerium-gadolinium oxalate, *J. Am. Ceram. Soc.*, **65**, [12], 606 – 609, (1982).

[94] Park, Z.H., Shin, H.S., Lee, B.K., Cho, S.H.: Particle size control of barium titanate prepared from barium titanyl oxalate, *J. Am. Ceram. Soc.*, **80**, [6], 1599 – 1604, (1997).

[95] Shen, A.-T., Lee, Y.-S., Sungyu, N.-K.: Characterization of calcium lanthanum oxalate powders coprecipitated from different binary solvent mixtures, *J. Am. Ceram. Soc.*, **76**, [6], 1466 – 1472, (1993).

[96] Shter, G.E., Grader, G.S.: YBCO oxalate coprecipitation in alcoholic solutions, *J. Am. Ceram. Soc.*, **77**, [6], 1436 – 1440, (1994).

[97] Vaidya, S., Ahmad, T., Agarwal, S., Ganguli, A.K.: Nanocrystalline oxalate/carbonate precursors of ce and zr and their decompositions to CeO_2 and ZrO_2 nanoparticles, *J. Am. Ceram. Soc.*, **90**, [3], 863 – 869, (2007).

[98] Vasylkiv, O., Sakka, Y.: Nonisothermal synthesis of yttria – stabilized zirconia nanopowder through oxalate processing: I, characteristics of Y-Zr oxalate synthesis and its decomposition, *J. Am. Ceram. Soc.*, **83**, [9], 2196 – 2202, (2000).

[99] Cernea, M., Chirtop, E., Neacsu, D., Pasuk, I., Iordanescu, S.: Preparation of $BaTi_4O_9$ from oxalates, *J. Am. Ceram. Soc.*, **85**, [2], 499 – 503, (2002).

[100] Gallagher, P.K., Schrey, F.: Preparation and thermal analysis of mixed magnesium-manganese-iron oxalates and hydrated oxides, *J. Am. Ceram. Soc.*, **47**, [9], 434 – 437, (1964).

[101] Kong, L., Karatchevtseva, I., Blackford, M.G., Scales, N., Triani, G.: Aqueous chemical synthesis of $Ln_2Sn_2O_7$ pyrochlore – structured ceramics, *J. Am. Ceram. Soc.*, **96**, [9], 2994 – 3000, [2013).

[102] Malghe, Y.S.: Nanosized $PbZrO_3$ powder from oxalate precursor: Microwave-aided synthesis and thermal characterization, *J. Am. Ceram. Soc.*, **92**, [9], 2155 – 2158, (2009).

[103] Xiu, Z., Li, J.-G., Li, X., Huo, D., Sun, X., Ikegami, T., Ishigaki, T.: Nanocrystalline scandia powders via oxalate precipitation: the effects of solvent and solution pH, *J. Am. Ceram. Soc.*, **91**, [2], 603 – 606, (2008).

[104] Schildermans, I., Knaepen, E., Nouwen, R., Van Bael, M.K., Vanhoyland, G., Mullens, J., Yperman, J., Franco, D., Van Poucke, L.C.: Thermal treatment of a Y-123 precursor prepared using the hydroxide q co-precipitation method, *Int. J. Inorg. Mater.,* **1**, 351 – 355, (1999).

[105] Skirius, S.A., Mathias, H.H.G., Hascicek, Y.S., Shankle, G., Clark, R.J.: Synthesis of high temperature superconducting ceramics by oxalate coprecipitatation from non-aqueous solvents, *Appl. Supercond.,* **2**, [2], 127 – 133, (1994).

[106] Baes, C.F.J., Mesmer, R.E.: The hydrolysis of cations. Krieger Publishing Company: Malabar, FL, 1976.

[107] Levinson, L.M., Philipp, H.R.: Physics of metal – oxide varistors, *J. Appl. Phys.,* **46**, [3], 1332 – 1341, (1975).

[108] Clarke, D.R.: Varistor ceramics, *J. Am. Ceram. Soc.*, **82**, [3], 485 – 502, (1999).

[109] Fuerstenau, D.W., Lutch, J.J., De, A.: The effect of ball size on the energy efficiency of hybrid high-pressure roll mill/ball mill grinding, *Powder Technol.*, **105**, 199 – 204, (1999).

[110] Sato, K., Li, J. – G., Kamiya, H., Ishigaki, T., Ultrasonic dispersion of tio2 nanoparticles in aqueous suspension, *J. Am. Ceram. Soc.*, **91**, (8], 2481 – 2487, (2008).

[111] Zheng, J., Harris, C.C., Somasundaran, P., The effect of additives on stirred media milling of limestone. *Powder Technol.*, **91**, [3], 173 – 179, (1997).

[112] He, M.Z., Wang, Y.M., Forssberg, E.: Parameter effects on wet ultrafine grinding of limestone through slurry rheology in a stirred media mill, *Powder Technol.*, **161**, [1], 10 – 21, (2006).

[113] Oettel, W., Husemann, K.: The effect of a grinding aid on comminution of fine limestone particle beds with single compressive load, *Int. J. Miner. Process.*, **74**, S239 – S248, (2004).

[114] Vemury, S., Pratsinis, S.E.: Self-preserving size distributions of agglomerates (vol 26, 175, 1995), *J. Aerosol Sci.*, **26**, [4], 701 – 701, (1995).

[115] Hennart, S.L.A., Wildeboer, W.J., van Hee, P., Meesters, G.M.H.: Identification of the grinding mechanisms and their origin in a stirred ball mill using population balances, *Chem. Eng. Sci.*, **64**, [19], 4123 – 4130, (2009).

[116] Mende, S., Stenger, F., Peukert, W., Schwedes, J.: Mechanical production and stabilization of submicron particles in stirred media mills, *Powder Technol.*, **132**, [1], 64 – 73, (2003).

[117] Stenger, F., Mende, S., Schwedes, J., Peukert, W.: Nanomilling in stirred media mills, *Chem. Eng. Sci.*, **60**, [16], 4557 – 4565, (2005).

[118] Kerr, M.C., Reed, J.S.: Comparative grinding kinetics and grinding energy during ball milling and attrition milling, *Am. Ceram. Soc. Bull.*, **71**, [12], 1809 – 1816, (1992).

[119] Kwade, A.: Wet comminution in stirred media mills – research and its practical application, *Powder Technol.,* **105**, 14 – 20, (1999).

[120] Kwade, A.: Mill selection and process optimization using a physical grinding model, *Int. J. Miner. Process.,* **74**, S93 – S101, (2004).

[121] Stender, H.H., Kwade, A., Schwedes, J.: Stress energy distribution in different stirred media mill geometries, *Int. J. Miner. Process.*, **74**, S103 – S117, (2004).

[122] Kwade, A., Blecher, L., Schwedes, J.: Motion and stress intensity of grinding beads in a stirred media mill. 2. Stress intensity and its effect on comminution. *Powder Technol.*, **86**, [1], 69 – 76, (1996).

[123] Blecher, L., Kwade, A., Schwedes, J.: Motion and stress intensity of grinding beads in a stirred media mill. 1. Energy density distribution and motion of single grinding beads, *Powder Technol.,* **86**, [1], 59 – 68, (1996).

[124] Adam, J., Drumm, R., Klein, G., Veith, M.: Milling of zirconia nanoparticles in a stirred media mill, *J. Am. Ceram. Soc.*, **91**, (9], 2836 – 2843, (2008).

[125] Adair, J.H., Shrout, T.R., Messing, G.L., Pecor, T.M., Mandanas, M.M.: Dynamic control and enhanced chemical milling of ceramics to submicron particle sizes. US 6,415,996 BI, (2002).

[126] Russel, W.B., Saville, D.A., Schowalter, W.R.: Colloidal dispersions. Cambridge University Press, Cambridge, 1999.

[127] Israelachvili, J., Intermolecular and surface forces. 2nd ed.; Academic Press: London, 1992.

[128] French, R.H.: Origins and applications of london dispersion forces and hamaker constants in ceramics, *J. Am. Ceram. Soc.*, **83**, [9], 2117 – 2146, (2000).

[129] Ackler, H.D., French, R.H., Chiang, Y.M.: Comparisons of hamaker constants for ceramic systems with intervening vacuum or water: from force laws and physical properties, *J. Colloid Interf. Sci.*, **179**, [2], 460 – 469, (1996).

[130] French, R.H., Cannon, R.M., Denoyer, L.K., Chiang, Y.M.: Full spectral calculation of nonretarded hamaker constants for ceramic systems from interband transition strengths, *Solid State Ionics*, **75**, 13 – 33, (1995).

[131] French, R.H., Scheu, C., Duscher, G., Mullejans, H., Hoffmann, M.J., Cannon, R.M.: Interfacial electronic structure and full spectral hamaker constants of Si_3N_4 intergranular films from VUV and SR-veel spectroscopy, *Mater. Res. Soc. Symp. P,* **357**, 243 – 258, (1995).

[132] Hough, D.B., White, L.R.: The calculation of hamaker constants from lifshitz theory with applications to wetting phenomena, *Adv. Colloid. Interfac.*, **14**, [1], 3 – 41, (1980).

[133] Bergstrom, L.: Hamaker constants of inorganic materials. *Adv. Colloid. Interfac.*, **70**, 125 – 169, (1997).

[134] Bergstrom, L., Meurk, N., Arwin, H., Rowcliffe, D.J.: Estimation of hamaker constants of ceramic materials from optical data using lifshitz theory, *J. Am. Ceram. Soc.*, **79** [2], 339 – 348, (1996).

[135] Parsegian, V.A.: Van der Waals forces: A handbook for biologists, chemists, engineers, and physicists. Cambridge University Press: Cambridge, 2006.

[136] Rosenholm, J.B., Peiponen, K.E., Gornov, E.: Materials cohesion and interaction forces, *Adv. Colloid Interfac.*, **141**, [1 – 2], 48 – 65, (2008).

[137] Kamiya, H., Iijima, M.: Surface modification and characterization for dispersion stability of inorganic nanometer – scaled particles in liquid media, *Sci. Technol. Adv. Mat.,* **11**, [4], (2010).

[138] Vayssieres, L.: On the effect of nanoparticle size on water – oxide interfacial chemistry, *J. Phys. Chem. C.,* **113**, [12], 4733 – 4736, (2009).

[139] Kosmulski, M.: Compilation of PZC and IEP of sparingly soluble metal oxides and hydroxides from literature, *Adv. Colloid Interfac.*, **152**, [1 – 2], 14 – 25, (2009).

[140] Kosmulski, M.: The pH-dependent surface charging and points of zero charge: IV. Update and new approach, *J. Colloid Interf. Sci.*, **337**, [2], 439 – 448, (2009).

[141] Kosmulski, M.: The pH-dependent surface charging and points of zero charge: V. Update, *J. Colloid Interf. Sci.*,**53**, [1], 1 – 15, (2011).

[142] Kosmulski, M.: IEP as a parameter characterizing the pH-dependent surface charging of materials other than metal oxides, *Adv. Colloid Interfac.,* **171**, 77 – 86, (2012).

[143] Tejuca, L.G., Rochester, C.H., Fierro, J.L.G., Tascon, J.M.D.: Infrared spectroscopic study of the adsorption of pyridine, carbon-monoxide and carbon-dioxide on the perovskite-type oxides $LaMO_3$, *J. Chem. Soc. Farad. T. 1*, **80**, 1089 – 1099, (1984).

[144] Tejuca, L.G., Fierro, J.L.G., Tascon, J.M.D.: Structure and reactivity of perovskite-type oxides, *Adv. Catal.,* **36**, 237 – 328, (1989).

[145] Hotze, E.M., Phenrat, T., Lowry, G.V.: Nanoparticle aggregation: challenges to understanding transport and reactivity in the environment, *J. Environ. Qual.*, **39**, [6], 1909 – 1924, (2010).

[146] Liu, X., Chen, G., Su, C.: Effects of material properties on sedimentation and aggregation of titanium dioxide nanoparticles of anatase and rutile in the aqueous phase, *J. Colloid Interf. Sci.*, **363**, [1], 84 – 91, (2011).

[147] Fazio, S., Guzman, J., Colomer, M., Salomoni, A., Moreno, R.: Colloidal stability of nanosized titania aqueous suspensions, *J. Eur. Ceram. Soc.*, **28**, [11], 2171 – 2176, (2008).

[148] Wang, N., Hsu, C., Zhu, L., Tseng, S., Hsu, J.P.: Influence of metal oxide nanoparticles concentration on their zeta potential, *J. Colloid Interf. Sci.*, **407**, 22 – 28, (2013).

[149] Jailani, S., Franks, G.V., Healy, T.W.: Zeta potential of nanoparticle suspensions: effect of electrolyte concentration, particle size, and volume fraction, *J. Am. Ceram. Soc.*, **91**, [4], 1141 – 1147, (2008).

[150] Butt, H.-J., Graf, K., Kappl, M.: Physics and chemistry of interfaces. Wiley – VCH: Weinheim, Germany, 2013.

[151] Lobbus, M., Sonnfeld, J., van Leeuwen, H. P., Vogelsberger, W., Lyklema, J.: An improved method for calculating zeta potentials from measurements of the electrokinetic sonic amplitude, *J. Colloid Interf. Sci.*, **229**, [1], 174 – 183, (2000).

[152] Morrison, I.D., Ross, S.: Colloidal dispersions suspensions, emulsions, and foams. Wiley – Interscience, New York, 2002.

[153] Obrien, R.W., Cannon, D.W., Rowlands, W.N.: Electroacoustic determination of particle size and zeta potential, *J. Colloid Interf. Sci.*, **173**, [2], 406 – 418, (1995).

[154] Dukhin, A.S., Goetz, P.J.: Acoustic and electroacoustic spectroscopy characterizing concentrated dispersions emulsions, *Adv. Colloid. Interfac.*, **92**, [1 – 3], 73 – 132, (2001).

[155] Dukhin, A.S., Ohshima, H., Shilov, V.N., Goetz, P.J.: Electroacoustics for concentrated dispersions, *Langmuir*, **15**, [10], 3445 – 3451, (1999).

[156] Dukhin, A.S., Goetz, P.J.: Characterization of aggregation phenomena by means of acoustic and electroacoustic spectroscopy, *Colloid. Surface. A*, **144**, [1 – 3], 49 – 58, (1998).

[157] Cruz, R.C.D., Reinshagen, J., Oberacker, R., Segadaes, A.M., Hoffmann, M.J.: Electrical conductivity and stability of concentrated aqueous alumina suspensions, *J. Colloid Interf. Sci.*, **286**, [2], 579 – 588, (2005).

[158] Henry, D.C.: The cataphoresis of suspended particles. part I. the equation of cataphoresis, *P. R. Soc. Lond. A – Conta.,* **133**, [821], 106 – 129, (1931).

[159] Obrien, R.W., White, L.R.: Electrophoretic mobility of a spherical colloidal particle, *J. Chem. Soc. Farad. T. 2*, **74**, 1607 – 1626, (1978).

[160] Ohshima, H., Healy, T.W., White, L.R.: Approximate analytic expressions for the electrophoretic mobility of spherical colloidal particles and the conductivity of their dilute suspensions, *J. Chem. Soc. Farad. T. 2*, **79**, 1613 – 1628, (1983).

[161] Makino, K., Ohshima, H.: Electrophoretic mobility of a colloidal particle with constant surface charge density, *Langmuir*, **26**, [23], 18016 – 18019, (2010).

[162] Abbas, Z., Labbez, C., Nordholm, S., Ahlberg, E.: Size-dependent surface charging of nanoparticles, *J. Phys. Chem. C,* **112**, [15], 5715 – 5723, (2008).

[163] Lyklema, J.: Fundamentals of interface and colloid science. Academic Press, London, 1995, Vol. II.

[164] He, Y.T., Wan, J.M., Tokunaga, T.: Kinetic stability of hematite nanoparticles: the effect of particle sizes, *J. Nanopart. Res.*, **10**, [2], 321 – 332, (2008).

[165] Holmberg, J.P., Ahlberg, E., Bergenholtz, J., Hassellov, M., Abbas, Z.: Surface charge and interfacial potential of titanium dioxide nanoparticles: experimental and theoretical investigations, *J. Colloid Interf. Sci.*, **407**, 168 – 176, (2013).

[166] Ridley, M.K., Machesky, M.L., Kubicki, J.D.: Anatase nanoparticle surface reactivity in NaCl media: A CD-music model interpretation of combined experimental and density functional theory studies, *Langmuir*, **29**, [27], 8572 – 8583, (2013).

[167] Suttiponparnit, K., Jiang, J., Sahu, M., Suvachittanont, S., Charinpanitkul, T., Biswas, P.: Role of surface area, primary particle size, and crystal phase on titanium dioxide nanoparticle dispersion properties, *Nanoscale Res. Lett.*, **6**, (2011).

[168] Zhou, D., Ji, Z., Jiang, X., Dunphy, D.R., Brinker, J., Keller, A.A.: Influence of material properties on TiO_2 nanoparticle agglomeration, *Plos One,* **8**, [11], (2013).

[169] Degreve, L., Lozadacassou, M., Sanchez, E., Gonzaleztovar, E.: Monte-carlo simulation for a symmetrical electrolyte next to a charged spherical colloid particle, *J. Chem. Phys.*, **98**, [11], 8905 – 8909, (1993).

[170] Zhang, Z., Fenter, P., Cheng, L., Sturchio, N.C., Bedzyk, M.J., Machesky, M.L., Wesolowski, D.J.: Model-independent X-ray imaging of adsorbed cations at the crystal-water interface, *Surf. Sci.,* **554**, [2 – 3], L95 – L100, (2004).

[171] Ridley, M.K., Machesky, M.L., Wesolowski, D.J., Palmer, D.A.: Surface complexation of neodymium at the rutile – water interface: A potentiometric and modeling study in NaCl media to 250 °C, *Geochim. Cosmochim. Ac.*, **69**, [1], 63 – 81, (2005).

[172] Ridley, M.K., Hiemstra, T., van Riemsdijk, W.H., Machesky, M.L.: Inner-sphere complexation of cations at the rutile-water interface: A concise surface structural interpretation with the CD and music model, *Geochim. Cosmochim. Ac.*, **73**, [7], 1841 – 1856, (2009).

[173] Zang, L., Liu, C.Y., Ren, X.M.: Adsorption of cations on TiO_2 particles – a method to determine the surface density of OH groups, *J. Chem. Soc. Chem. Comm.,* [16], 1865 – 1866, (1994).

[174] Zhang, Z., Fenter, P., Cheng, L., Sturchio, N.C., Bedzyk, M.J., Machesky, M.L., Anovitz, L.M., Wesolowski, D.J.: Zn^{2+} and Sr^{2+} adsorption at the TiO_2 (110)-electrolyte interface: influence of ionic strength, coverage, and anions, *J. Colloid Interf. Sci.*, **295**, [1], 50 – 64, (2006).

[175] Zhang, Z., Fenter, P., Cheng, L., Sturchio, N.C., Bedzyk, M.J., Predota, M., Bandura, A., Kubicki, J.D., Lvov, S.N., Cummings, P.T., Chialvo, A.A., Ridley, M.K., Benezeth, P., Anovitz, L., Palmer, D.A., Machesky, M.L., Wesolowski, D.J.: Ion adsorption at the rutile-water interface: linking molecular and macroscopic properties, *Langmuir*, **20**, [12], 4954 – 4969, (2004).

[176] Zhang, Z., Fenter, P., Kelly, S.D., Catalano, J.G., Bandura, A.V., Kubicki, J.D., Sofo, J.O., Wesolowski, D.J., Machesky, M.L., Sturchio, N.C., Bedzyk, M.J.: Structure of hydrated Zn^{2+} at the rutile TiO_2 (110)-aqueous solution interface: comparison of X-ray standing wave, X-ray absorption spectroscopy, and density functional theory results, *Geochim. Cosmochim. Ac.*, **70**, [16], 4039 – 4056, (2006).

[177] Machesky, M.L., Wesolowski, D.J., Palmer, D.A., Ridley, M.K.: On the temperature dependence of intrinsic surface protonation equilibrium constants: an extension of the revised music model, *J. Colloid Interf. Sci.*, **239**, [2], 314 – 327, (2001).

[178] Ridley, M.K., Hiemstra, T., Machesky, M.L., Wesolowski, D.J., van Riemsdijk, W.H.: Surface speciation of yttrium and neodymium sorbed on rutile: interpretations using the charge distribution model, *Geochim. Cosmochim. Ac.*, **95**, 227 – 240, (2012).

[179] Ring, T.A.: Fundamentals of ceramic powder processing and synthesis. Academic Press, San Diego, 1996.

[180] Kosmulski, M., Prochniak, P., Rosenholm, J.B.: Electroacoustic study of titania at high concentrations of 1 – 2, 2 – 1 and 2 – 2 electrolytes, *Colloid. Surface. A*, **345**, [1 – 3], 106 – 111, (2009).

[181] Hiemstra, T., Van Riemsdijk, W.H., Bolt, G.H.: Multisite proton adsorption modeling at the solid/solution interface of (hydr)oxides: A new approach I. model description and evaluation of intrinsic reaction constants, *J. Colloid Interf. Sci.*, **133**, [1], 91 – 104, (1989).

[182] Hiemstra, T., De Wit, J.C.M., Van Riemsdijk, W.H.: Multisite proton adsorption modeling at the solid/solution interface of (hydr)oxides: A new approach II. application to various important (hydr)oxides, *J. Colloid Interf. Sci.*, **133**, [1], 105 – 117, (1989).

[183] Hiemstra, T., Van Riemsdijk, W.H.: Physical chemical interpretation of primary charging behavior of metal (hydr)oxides, *Colloids. Surface.*, **59**, 7 – 25, (1991).

[184] Hiemstra, T., Venema, P., Van Riemsdijk, W.H.: Intrinsic proton affinity of reactive surface groups of metal (hydr)oxides: the bond valence principle, *J. Colloid Interf. Sci.*, **184**, 680 – 692, (1996).

[185] Hiemstra, T., Van Riemsdijk, W.H.: A surface structural approach to ion adsorption: the charge distribution model, *J. Colloid Interf. Sci.*, **179**, 488 – 508, (1996).

[186] Stachowicz, M., Hiemstra, T., van Riemsdijk, W.H.: Surface speciation of As(III) and As(V) in relation to charge distribution, *J. Colloid Interf. Sci.*, **302**, [1], 62 – 75, (2006).

[187] Wesolowski, D.J., Machesky, M.L., Palmer, D.A., Anovitz, L.M.: Magnetite surface charge studies to 290 °C from *in situ* pH titrations, *Chem. Geol.*, **167**, [1 – 2], 193 – 229, (2000).

[188] Ridley, M.K., Machesky, M.L., Kubicki, J.D.: Experimental study of strontium adsorption on anatase nanoparticles as a function of size with a density functional theory and CD model interpretation, *Langmuir*, **31**, [2], 703 – 713, (2015).

[189] Ridley, M.K., Machesky, M.L., Wesolowski, D.J., Palmer, D.A.: Modeling the surface complexation of calcium at the rutile-water interface to 250 °C, *Geochim. Cosmochim. Ac.*, **68**, [2], 239 – 251, (2004).

[190] Zebardast, H.R., Pawlik, M., Rogak, S., Asselin, E.: Potentiometric titration of hematite and magnetite at elevated temperatures using a ZrO_2-based pH probe, *Colloid. Surface. A*, **444**, 144 – 152, (2014).

[191] Machesky, M.L., Wesolowski, D.J., Palmer, D.A., Ichiro-Hayashi, K.: Potentiometric titrations of rutile suspensions to 250 °C, *J. Colloid Interf. Sci.*, **200**, [2], 298 – 309, (1998).

[192] Palmer, D.A., Machesky, M.L., Benezeth, P., Wesolowski, D.J., Anovitz, L.M., Deshon, J.C.: Adsorption of ions on zirconium oxide surfaces from aqueous solutions at high temperatures, *J. Solution Chem.*, **38**, [7], 907 – 924, (2009).

[193] Bunker, B.C.: Formal charge model for predicting structures, acid-base, and ion exchange properties of mixed oxides, In San Francisco, CA, 1997.

[194] Hanawa, T., Kon, M., Doi, H., Ukai, H., Murakami, K., Hamanaka, H., Asaoka, K.: Amount of hydroxyl radical on calcium-ion-implanted titanium and point of zero charge of constituent oxide of the surface-modified layer, *J. Mater. Sci.*, **9**, [2], 89 – 92, (1998).

[195] Lencka, M.M., Riman, R.E.: Thermodynamic modeling of hydrothermal synthesis of ceramic powders, *Chem. Mater.*, **5**, 61 – 70, (1993).

[196] Wang, X.Y., Lu, S.W., Lee, B.I., Mann, L.A.: Dispersion and aging behavior of $BaTiO_3$ and PZT in water, *Mater. Res. Bull.,* **35**, [14 – 15], 2555 – 2563, (2000).

[197] Wendelbo, R., Akporiaye, D.E., Karlsson, A., Plassen, M., Olafsen, A.: Combinatorial hydrothermal synthesis and characterisation of perovskites, *J. Eur. Ceram. Soc.*, **26**, [6], 849 – 859, (2006).

[198] Hayun, S., Navrotsky, A.: Formation enthalpies and heat capacities of rear earth titanates: RE_2TiO_5 (*RE*=La, nd and Gd), *J. Solid State Chem.*, **187**, 70 – 74, (2012).

[199] Modeshia, D.R., Walton, R.I.: Solvothermal synthesis of perovskites and pyrochlores: crystallisation of functional oxides under mild conditions, *Chem. Soc. Rev.*, **39**, [11], 4303 – 4325, (2010).

[200] Sahu, S.K., Maram, P.S., Navrotsky, A.: Thermodynamics of nanoscale calcium and strontium titanate perovskites, *J. Am. Ceram. Soc.*, **96**, [11], 3670 – 3676, (2013).

[201] Studart, A.R., Amstad, E., Gauckler, L.J.: Colloidal stabilization of nanoparticles in concentrated suspensions, *Langmuir*, **23**, 1081 – 1090, (2007).

[202] Ata, M.S., Liu, Y., Zhitomirsky, I.: A review of new methods of surface chemical modification, dispersion and electrophoretic deposition of metal oxide particles, *RSC Advances*, **4**, [43], 22716 – 22732, (2014).

[203] Raj, P.M., Cannon, W.R.: Electrosteric stabilization mechanisms in nonaqueous high solids loading dispersions. In: Polymers in particulate systems properties and applications, Hackley, V.A., Somasundaran, P., Lewis, J.A., Eds. Marcel Dekker, New York, 2002; Vol. 104, 27 – 61.

[204] Claesson, P.M., Poptoshev, E., Blomberg, E., Dedinaite, A.: Polyelectrolyte-mediated surface interactions, *Adv. Colloid. Interface. Sci.*, **114 – 115**, 173 – 187, (2005).

[205] Tseng, W.J., Wang, S.-R.: Dispersion and rheology of $BaTiO_3$ nanoparticles in ethanol-isopropanol solvents, *J. Electroceram.,* **18**, [3 – 4], 197 – 204, (2007).

[206] Shen, Z.G., Chen, J.F., Zou, H.K., Yun, J.: Dispersion of nano-sized aqueous suspensions of barium titanate with ammonium polyacrylate, *J. Colloid Interf. Sci.*, **275**, [1], 158 – 164, (2004).

[207] Gomez-Yanez, C., Balmori-Ramirez, H., Martinez, F.: Colloidal processing of $BaTiO_3$ using ammonium polyacrylate as dispersant, *Ceram. Int.*, **26**, [6], 609 – 616, (2000).

[208] Liu, G., Zhang, D., Button, T.W.: Preparation of concentrated barium titanate suspensions incorporating nano-sized powders, *J. Eur. Ceram. Soc.*, **30**, [2], 171 – 176, (2010).

[209] Lu, K., Kessler, C.S., Davis, R.M.: Optimization of a nanoparticle suspension for freeze casting, *J. Am. Ceram. Soc.*, **89**, [8], 2459 – 2465, (2006).

[210] Tseng, W.J., Tzeng, F.: Effect of ammonium polyacrylate on dispersion and rheology of aqueous ito nanoparticle colloids, *Colloid. Surface A*, **276**, [1 – 3], 34 – 39, (2006).

[211] Liufu, S.C., Mao, H.N., Li, Y.P.: Adsorption of poly(acrylic acid) onto the surface of titanium dioxide and the colloidal stability of aqueous suspension, *J. Colloid. Interf. Sci.*, **281**, [1], 155 – 163, (2005).

[212] Liufu, S.C., Xiao, H.N., Li, Y.P.: Adsorption of polyelectrolyte on the surface of ZnO nanoparticles and the stability of colloidal dispersions, *Chinese Sci. Bull.*, **50**, [15], 1570 – 1575, (2005).

[213] Blanco-Lopez, M.C., Rand, B., Riley, F.L.: Polymeric stabilisation of aqueous suspensions of barium titanate. part II. effect of polyelectrolyte concentration, *J. Eur. Ceram. Soc.*, **20**, 1587 – 1594, (2000).

[214] Davies, J., Binner, J.G.P.: The role of ammonium polyacrylate in dispersing concentrated alumina suspensions, *J. Eur. Ceram. Soc.*, **20**, [10], 1539 – 1553, (2000).

[215] Das, K.K., Somasundaran, P.: Flocculation – dispersion characteristics of alumina using a wide molecular weight range of polyacrylic acids, *Colloid. Surface. A*, **223**, [1 – 3], 17 – 25, (2003).

[216] Cesarano, J., Aksay, I.A.: Processing of highly concentrated aqueous alpha-alumina suspensions stabilized with poly-electrolytes, *J. Am. Ceram. Soc.*, **71**, [12], 1062 – 1067, (1988).

[217] Ohtsuka, H., Mizutani, H., Iio, S., Asai, K., Kiguchi, T., Satone, H., Mori, T., Tsubaki, J.: Effects of sintering additives on dispersion properties of Al_2O_3 slurry containing polyacrylic acid dispersant, *J. Eur. Ceram. Soc.*, **31**, [4], 517 – 522, (2011).

[218] Traiphol, N., Suntako, R., Chanthornthip, K.: Roles of polymeric dispersant charge density on lead zirconate titanate aqueous processing, *Ceram. Int.*, **36**, [7], 2147 – 2153, (2010).

[219] Pedersen, H.G., Bergstrom, L.: Forces measured between zirconia surfaces in poly(acrylic acid) solutions, *J. Am. Ceram. Soc.*, **82**, [5], 1137 – 1145, (1999).

[220] Sato, K., Kondo, S., Tsukada, M., Ishigaki, T., Kamiya, H.: Influence of solid fraction on the optimum molecular weight of polymer dispersants in aqueous TiO_2 nanoparticle suspensions, *J. Am. Ceram. Soc.*, **90**, [11], 3401 – 3406, (2007).

[221] Tripathy, S.S., Raichur, A.M.: Dispersibility of barium titanate suspension in the presence of polyelectrolytes: A review, *J. Disper. Sci. Technol.*, **29**, [2], 230 – 239, (2008).

[222] Manning, G.S.: Counterion binding in polyelectrolyte theory, *Accounts Chem. Res.*, **12**, [12], 443 – 449, (1979).

[223] Manning, G.S., Ray, J.: Counterion condensation revisited, *J. Biomol. Struct. Dyn.*, **16**, [2], 461 – 476, (1998).

[224] Drifford, M., Delsanti, M.: Polyelectrolyte solutions with multivalent added salts: Stability, structure and dynamics. In: Physical chemistry of polyelectrolytes, Radeva, T., Ed. Marcel Dekker, Inc.: New York, 2001; 135 – 161.

[225] Miyajima, T.: Metal complexation in polyelectrolyte solutions. In: Physical chemistry of polyelectrolytes, Radeva, T., Ed. Marcel Dekker, Inc.: New York, 2001; 829 – 874.

[226] Abraham, T.: Effects of divalent salt on adsorption kinetics of a hydrophobically modified polyelectrolyte at the neutral surface-aqueous solution interface, *Polymer*, **43**, [3], 849 – 855, (2002).

[227] Bell, N.S., Sindel, J., Aldinger, F., Sigmund, W.M.: Cation-induced collapse of low-molecular-weight polyacrylic acid in the dispersion of barium titanate, *J. Colloid Interf. Sci.*, **254**, [2], 296 – 305, (2002).

[228] Fleer, G.J., Stuart, M.A.C., Scheutjens, J.M.H.M., Cosgrove, T., Vincent, B.: Polymers at interfaces, Chapman and Hall, London, 1993.

[229] Tadros, T.: Polymeric surfactants in disperse systems, *Adv. Colloid Interfac.*, **147 – 48**, 281 – 299, (2009).

[230] Tadros, T.: Interaction forces between adsorbed polymer layers, *Adv. Colloid Interfac.*, **165**, [2], 102 – 107, (2011).

[231] Klimkevicius, V., Graule, T., Makuska, R.: Effect of structure of cationic comb copolymers on their adsorption and stabilization of titania nanoparticles, *Langmuir*, **31**, [7], 2074 – 2083, (2015).

[232] Rhodes, S.K., Lambeth, R.H., Gonzales, J., Moore, J.S., Lewis, J.A.: Cationic comb polymer superdispersants for colloidal silica suspensions, *Langmuir*, **25**, [12], 6787 – 6792, (2009).

[233] Mewis, J., Vermant, J.: Rheology of sterically stabilized dispersions and lattices, *Prog. Org. Coat.*, **40**, 111 – 117, (2000).

[234] Tadros, T.: Interaction forces between particles containing grafted or adsorbed polymer layers, *Adv. Colloid Interfac.*, **104**, 191 – 226, (2003).

[235] Yoshikawa, J., Lewis, J.A., Chun, B.-W.: Comb polymer architecture, ionic strength, and particle size effects on the $BaTiO_3$ suspension stability, *J. Am. Ceram. Soc.*, **92**, [1], S42 – S49, (2009).

[236] Flatt, R.J., Schober, I., Raphael, E., Plassard, C., Lesniewska, E.: Conformation of adsorbed comb copolymer dispersants, *Langmuir*, **25**, [2], 845 – 855, (2009).

[237] Marchon, D., Sulser, U., Eberhardt, A., Flatt, R.J.: Molecular design of comb-shaped polycarboxylate dispersants for environmentally friendly concrete, *Soft. Matter.,* **9**, [45], 10719 – 10728, (2013).

[238] Ran, Q., Qiao, M., Liu, J.: Influence of Ca^{2+} on the performance of poly(acrylic acid)-g-poly(ethylene glycol) comb-like copolymers in cement suspensions, *Iran. Polym. J.,* **23**, [9[, 663 – 669, (2014).

[239] Ran, Q., Somasundaran, P., Miao, C., Liu, J., Wu, S., Shen, J.: Effect of the length of the side chains of comb-like copolymer dispersants on dispersion and rheological properties of concentrated cement suspensions, *J. Colloid. Interf. Sci.*, **336**, [2], 624 – 633, (2009).

[240] Kirby, G.H., Lewis, J.A.: Comb polymer architecture effects on the rheological property evolution of concentrated cement suspensions, *J. Am. Ceram. Soc.*, **87**, [9], 1643 – 1652, (2004).

[241] Chen, L.P., Wu, H.H., Hsu, K.C.: Synthesis and application of an anionic water-soluble copolymer as a dispersant for barium titanate slurries, *J. Appl. Polym. Sci.*, **98**, [1], 109 – 115, (2005).

[242] Sakar-Deliormanli, A., Celik, E., Polat, M.: Influence of dispersing agents on the solubility of perovskites in water, *J. Disper. Sci. Technol.*, **30**, [5], 704 – 711, (2009).

[243] Hidber, P.C., Graule, T.J., Gauckler, L.J.: Influence of the dispersant structure on properties of electrostatically stabilized aqueous alumina suspensions, *J. Eur. Ceram. Soc.*, **17**, 239 – 249, (1997).

[244] Studart, A.R., Amstad, E., Gauckler, L.J.: Colloidal stabilization of nanoparticles in concentrated suspensions, *Langmuir*, **23**, [3], 1081 – 1090, (2007).

[245] Tsai, C.-J., Chen, C.-N., Tseng, W.J.: Rheology, structure, and sintering of zirconia suspensions with pyrogallol – poly(ethylene glycol) as polymeric surfactant, *J. Eur. Ceram. Soc.*, **33**, [15 – 16], 3177 – 3184, (2013).

[246] Lee, H., Dellatore, S.M., Miller, W.M., Messersmith, P.B.: Mussel-inspired surface chemistry for multifunctional coatings, *Science*, **318**, [5849], 426 – 430, (2007).

[247] Amstad, E., Gehring, A.U., Fischer, H., Nagaiyanallur, V.V., Hahner, G., Textor, M., Reimhult, E.: Influence of electronegative substituents on the binding affinity of catechol-derived anchors to Fe_3O_4 nanoparticles, *J. Phys. Chem. C.,* **115**, [3], 683 – 691, (2011).

[248] Amstad, E., Gillich, T., Bilecka, I., Textor, M., Reimhult, E.: Ultrastable iron oxide nanoparticle colloidal suspensions using dispersants with catechol-derived anchor groups, *Nano Lett.,* **9**, [12], 4042 – 4048, (2009).

[249] Gillich, T., Benetti, E.M., Rakhmatullina, E., Konradi, R., Li, W., Zhang, A., Schluter, A.D., Textor, M.: Self-assembly of focal point oligo-catechol ethylene glycol dendrons on titanium oxide surfaces: adsorption kinetics, surface characterization, and nonfouling properties, *J. Am. Chem. Soc.*, **133**, [28], 10940 – 10950, (2011).

[250] Malisova, B., Tosatti, S., Textor, M., Gademann, K., Zurcher, S.: Poly(ethylene glycol) adlayers immobilized to metal oxide substrates through catechol derivatives: influence of assembly conditions on formation and stability, *Langmuir*, **26**, [6], 4018 – 4026, (2010).

[251] Bondietti, G., Sinniger, J., Stumm, W.: The reactivity of Fe(III) (hydr)oxides – effects of ligands in inhibiting the dissolution, *Colloid. Surface. A*, **79**, [2 – 3], 157 – 167, (1993).

[252] Biber, M.V., Afonso, M.D., Stumm, W.: The coordination chemistry of weathering .IV. inhibition of the dissolution of oxide minerals, *Geochim. Cosmochim. Ac.*, **58**, [9], 1999 – 2010, (1994).

[253] Eick, M.J., Peak, J.D., Brady, W.D.: The effect of oxyanions on the oxalate – promoted dissolution of goethite, *Soil Sci. Soc. Am. J.*, **63**, [5], 1133 – 1141, (1999).

[254] Pang, C.L., Lindsay, R., Thornton, G.: Structure of clean and adsorbate-covered single-crystal rutile TiO_2 surfaces, *Chem. Rev.,* **113**, [6], 3887 – 3948, (2013).

[255] Wu, H., Jiang, D., Cai, P., Rong, X., Huang, Q.: Effects of low-molecular-weight organic ligands and phosphate on adsorption of pseudomonas putida by clay minerals and iron oxide, *Colloid. Surface B*, **82**, [1], 147 – 151, (2011).

[256] Studart, A.R., Pandolfelli, V.C., Tervoort, E., Gauckler, L.J., Selection of dispersants for high-alumina zero-cement refractory castables, *J. Eur. Ceram. Soc.*, **23**, [7], 997 – 1004, (2003).

[257] Tanurdjaja, S., Tallon, C., Scales, P.J., Franks, G.V.: Influence of dispersant size on rheology of non-aqueous ceramic particle suspensions, *Adv. Powder. Technol.*, **22**, [4], 476 – 481, (2011).

[258] Kimel, R.A., Adair, J.H.: Aqueous degradation and chemical passivation of yttria-tetragonally- stabilized zirconia at 25 °C, *J. Am. Ceram. Soc.*, **85**, [6], 1403 – 1408, (2002).

[259] Adair, J.H., Crampo, J., Mandanas, M.M., Suvaci, E.: The role of material chemistry in processing $BaTiO_3$ in aqueous suspensions, *J. Am. Ceram. Soc.*, **89**, [6], 1853 – 1860, (2006).

[260] Kettler, R.M., Palmer, D.A., Wesolowski, D.J.: Dissociation quotients of oxalic – acid in aqueous sodium – chloride media to 175 °C, *J. Solution. Chem.*, **20**, [9], 905 – 927, (1991).

[261] Janos, P.: Determination of stability constants of metal complexes from ion chromatographic measurements. *J. Chromatogr.*, **641**, 229 – 234, (1993).

[262] Kundin, J., Yu, C.-J., Conradt, R., Emmerich, H.: Simulation of adsorption processes on the glass surface in aqueous solutions containing oxalic acid, *Comp. Mater. Sci.*, **49**, [1], 88 – 98, (2010).

[263] Degenhardt, J., McQuillan, A.J.: Mechanism of oxalate ion adsorption on chromium oxide – hydroxide from pH dependence and time evolution of ATR – IR spectra, *Chem. Phys. Lett.*, **311**, [3 – 4], 179 – 184, (1999).

[264] Filius, J.D., Hiemstra, T., Van Riemsdijk, W.H.: Adsorption of small weak organic acids on goethite: modeling of mechanisms, *J. Colloid. Interf. Sci.*, **195**, [2], 368 – 380, (1997).

[265] Del Nero, M., Galindo, C., Bucher, G., Georg, S., Mazan, V., Barillon, R.: Speciation of oxalate at corundum colloid – solution interfaces and its effect on colloid aggregation under conditions relevant to freshwaters, *Colloid. Surface. A*, **418**, 165 – 173, (2013).

[266] Hanaor, D., Michelazzi, M., Veronesi, P., Leonelli, C., Romagnoli, M., Sorrell, C.: Anodic aqueous electrophoretic deposition of titanium dioxide using carboxylic acids as dispersing agents, *J. Eur. Ceram. Soc.*, **31**, [6], 1041 – 1047, (2011).

[267] Hanaor, D., Michelazzi, M., Leonelli, C., Sorrell, C.C.: The effects of carboxylic acids on the aqueous dispersion and electrophoretic deposition of ZrO_2, *J. Eur. Ceram. Soc.*, **32**, [1], 235 – 244, (2012).

[268] Johnson, S.B., Brown, G.E., Healy, T.W., Scales, P.J.: Adsorption of organic matter at mineral/water interfaces. 6. effect of inner-sphere versus outer-sphere adsorption on colloidal stability, *Langmuir*, **21**, [14], 6356 – 6365, (2005).

[269] Erdemoglu, M., Sarikaya, M.: Effects of heavy metals and oxalate on the zeta potential of magnetite, *J. Colloid Interf. Sci.*, **300**, [2], 795 – 804, (2006).

[270] Coble, R.L., Burke, J.E.: Sintering in ceramics. The Macmillian Company, New York, 1963; Vol. 3.

[271] Thummler, F., Thomma, W.: The sintering process, *J. I. Met.*, **12**, 69 – 108, (1967).

[272] Burke, J.E., Rosolowski, J.H.: Sintering. Plenum Press, New York, 1976; Vol. 4.

[273] Coble, R.L.: Sintering crystalline solids .I. intermediate and final state diffusion models, *J. Appl. Phys.,* **32**, [5], 787, (1961).

[274] German, R.M.: Liquid phase sintering. Plenum Press, New York, 1985.

[275] Brinker, C.J., Scherer, G.W.: Sol-gel science, the physics and chemistry of sol-gel processing. Academic Press, New York, 1990.

[276] Ewsuk, K.G.: Consolidation of bulk ceramics. Butterworth – Heinemann: Greenwich, CT, 1993.

[277] Reed, J.S.: Introduction to the principles of ceramic processing. John Wiley & Sons, Inc., New York, 1995.

[278] Ewsuk, K.G.: Ceramics (processing). 4th ed.; John Wiley & Sons, Inc., 1993; Vol. 5.

[279] Richerson, D.W.: Modern ceramic engineering: Properties, processing, and use in design. 2nd ed.; Marcel Dekker, Inc., New York, 1992.

[280] Herring, C.: Surface tension as a motivation for sintering. McGraw – Hill Book Company, Inc.: New York, 1949.

[281] Kim, B.N., Hiraga, K., Morita, K., Yoshida, H.: Spark plasma sintering of transparent alumina, *Scripta Mater.,* **57**, [7], 607 – 610, (2007).

[282] Zhang, Y.F., Zhang, J.X., Lu, Q.M.: Synthesis of highly textured $Ca_3Co_4O_9$ ceramics by spark plasma sintering, *Ceram. Int.,* **33**, [7], 1305 – 1308, (2007).

[283] Matsubara, I., Funahashi, R., Takeuchi, T., Sodeoka, S.: Thermoelectric properties of spark plasma sintered $Ca_{2.75}Gd_{0.25}Co_4O_9$ ceramics, *J. Appl. Phys.*, **90**, [1], 462 – 465, (2001).

[284] Noudem, J.G., Kenfaui, D., Chateigner, D., Gomina, M.: Toward the enhancement of thermoelectric properties of lamellar $Ca_3Co_4O_9$ by edge-free spark plasma texturing, *Scripta Mater.,* **66**, [5], 258 – 260, (2012).

[285] Yang, D., Raj, R., Conrad, H.: Enhanced sintering rate of zirconia (3Y – TZP) through the effect of a weak DC electric field on grain growth, *J. Am. Ceram. Soc.*, **93**, [10], 2935 – 2937, (2010).

[286] Jeong, J.W., Han, J.H., Kim, D.Y.: Effect of electric field on the migration of grain boundaries in alumina, *J. Am. Ceram. Soc.*, **83**, [4], 915 – 918, (2000).